Ore Geology Reviews 109 (2019) 426–447

Contents lists available at ScienceDirect

Ore Geology Reviews

journal homepage: www.elsevier.com/locate/oregeorev

Occurrence of pyrites in sandstone-type uranium deposits: Relationships with uranium mineralization in the North Ordos Basin, China

Yin Chen[a,b,*], Ruoshi Jin[a,b], Peisen Miao[a,b], Jianguo Li[a,b], Hu Guo[a,b], Lulu Chen[a,b]

[a] Tianjin Center, China Geological Survey, Tianjin 300170, China
[b] Laboratory of Non-fossil Energy Minerals, Tianjin Center of China Geological Survey, Tianjin 300170, China

ARTICLE INFO

Keywords:
Sandstone-type uranium deposit
Pyrite
S isotopes
Calcite
Uranium mineralization
Ordos Basin

ABSTRACT

Large quantities of pyrite have been discovered near the ore-bearing segments of the sandstone-type uranium deposits in the North Ordos Basin. In this study, the electron probe microanalysis, scanning electron microscopy, and isotope geochemical analysis were used to systematically investigate the morphology, composition, and S isotopes of the pyrites in these deposits, and their genetic order relative to the other main altered minerals. Based on the regional tectonic evolutionary sequence of the basin, the relationships between the pyrites and uranium mineralization are discussed. Macroscopically, the pyrites were found to occur in lumpy, banded, disseminated, star-like or sheet-like form. Microscopically, they exist either as detrital grains or inside detrital grains, as idiomorphic grains, in colloidal or framboidal form, inside mica minerals, in banded or petaloid form, and in other forms related to biological cells or microorganisms. The $\delta^{34}S$‰ values in the pyrites are highly variable (−7.3‰ to −37.2‰), but principally in the proximity of −30‰, and display obvious biogenic origin. Taking into consideration the extremely low U contents in the pyrites and achavalites (iron selenide), the genetic order of the main altered minerals is determined as follows: detrital pyrites > clay mineral overgrowths > micritic calcites during the diagenetic stage; and achavalites > pyrites > coffinite/pitchblende > vanadium oxides > sparry calcites during the metallogenic stage. The broad presence of pyrites in the Jurassic Yan'an Formation during the basin's evolution provided detrital pyrites and organic detritus for the overlying formations. The Zhiluo Formation, host of the uranium mineralization, is also home to some primary spherical colloidal or framboidal pyrites. The Cretaceous was the main epigenetic uranium metallogenetic period as well as the main pyrite development period of the area. The pyrites, which are typically colloidal, have cemented the earlier framboidal pyrites and other minerals and are closely associated with the redox reaction related to uranium mineralization. In the Paleogene, uranium mineralization mainly occurred by the redox migration of early shallow deposits to, and fresh pyrites forming in deeper levels.

1. Introduction

The sandstones of Jurassic Zhiluo Formation in the North Ordos Basin are host to some of the most important sandstone-type uranium deposits in China, including the Nalinggou, Daying, and Zaohuohao uranium deposits (Cai et al., 2005; Deng et al., 2005; Li et al., 2007; Yang et al., 2008; Xue et al., 2010; Liu et al., 2012; Li et al., 2016; Wu et al., 2016; Zhang, 2016; Chen et al., 2017b; Hou et al., 2017; Zhang et al., 2017a). Although previous authors have identified the spatial paragenesis of uranium minerals and pyrites in these uranium deposits (Peng et al., 2006; Liu et al., 2006c; Chen et al., 2016; Wu et al., 2016), their exact mineral genetic sequences and interactions are not clearly identified. Some authors have suggested that, in a sandstone-type uranium deposit, the uranium enrichment in the redox fronts is the result of U^{6+} in an oxygenated water solution being reduced to U^{4+}, which subsequently precipitated and was concentrated into a deposit, with the uranium reducing agents including residual carbon debris or sulfides in the sandstone, especially pyrites, or reducing fluids from the deeper levels (Chen and Guo, 2007; Chen et al., 2017b; Jin et al., 2019). Much work has been conducted by previous authors with respect to the morphology, composition, S isotopes, and microstructure of the pyrites in solid sulfide deposits, unconformity-type and granite-type uranium deposits (Zhou et al., 2008; Gao et al., 2015; Qi et al., 2015; Skirrow et al., 2016; Zou et al., 2017; Hu et al., 2018; Manuel et al., 2018; Zhao et al., 2018a), but few researchers have taken a closer look at the category, composition, and genetic periods of the pyrites in sandstone-type uranium deposits, and their relationships with other altered minerals and uranium mineralization. Previously, many geologists have

* Corresponding author at: No. 4, Dazhigu 8th Road, Hedong, Tianjin 300170, China.
E-mail address: chenyinchain@sina.com (Y. Chen).

https://doi.org/10.1016/j.oregeorev.2019.03.037
Received 3 July 2018; Received in revised form 13 March 2019; Accepted 31 March 2019
Available online 04 May 2019
0169-1368/

focused on the S isotopic analysis of pyrite and C-H-O analysis of calcite to discuss the uranium ore-forming fluid (Cai et al., 2007; Wu et al., 2016; Zhao et al., 2018b). However, these isotopic works were the mixed results of several-stage altered minerals instead of the in-situ analysis, which would not represent the nature of ore-forming fluid in the uranium ore-forming process. In this paper, based on the analysis of the pyrite, the occurrence of major altered minerals will be obtained and relationship with uranium mineralization will be discussed, which is the basic background for the study of uranium ore-forming fluid.

Regarding the tectonic evolution of the North Ordos Basin, studies have been conducted through the analysis of field geological features, low-temperature chronological testing, and tectonic stress inversion, with focuses on tectonic stress transformation and its roles in the evolution of coal, oil or gas resources and related ore-forming fluids (Ren et al., 2007; Ding et al., 2011; Zhao et al., 2012; Yang et al., 2015; Wang, 2017). While some of these authors have realized the important roles played by tectonic evolution in the metallogenesis of sandstone-type uranium deposits (Sun et al., 2004; Deng et al., 2005; Liu et al., 2006a), few have considered how important minerals related to uranium mineralization (e.g., carbonates, pyrite, and uranium minerals) have manifested themselves during different tectonic evolutionary stages. In this paper, with reference to the findings of previous authors, the morphology, composition, and S isotopes of the pyrites in the sandstone-type uranium deposits in the North Ordos Basin are studied, and their paragenesis with other altered minerals are observed. The roles of pyrites in the uranium ore-forming process are also discussed in light of the regional tectonic evolution of the basin during the Mesozoic.

2. Regional geology

The study area lies in the North Ordos Basin (Fig. 1), in the northern flank of the slightly elevated end of the Northeastern Yimeng uplift. It borders the Yinshan orogen (the Ural and Daqingshan Mountains) to the north across the Hetao rift zone, and the Lüliang–Taihangshan orogen to the east. To its south is the Yishan slope, where the Ordos Basin becomes a wide, gentle slope zone (Deng et al., 2005; Yuan et al., 2007; Zhang et al., 2018 and references therein) (Fig. 1).

Exposed sedimentary formations in the area include the Early Cretaceous Ejinhoro and Dongsheng formations. The Cambrian–Ordovician and Permian–Jurassic depositional units exposed on the northern margin of the basin comprise the annular exposure of this area. The formations are generally gently dipping, with 1–10° SW dips (Akhtara et al., 2017). The Jurassic sediments, the main ore-bearing unit in the uranium deposits of the area, overlie the Triassic formation in unconformity resulting from the Indosinian Movement II (Qiu et al., 2014; Akhtara et al., 2017), and underlie the Cretaceous formation in angular unconformity resulting from the Yanshanian Movement A (Yuan et al., 2007; Zhao et al., 2015) (Table 1). The Cretaceous underwent extensive elevation–denudation in the later stage as a result of the Yanshannian Movement B and the Himalayan Movement (Liu et al., 2006a; Chen et al., 2016).

The Middle Jurassic Zhiluo Formation, which is the main uranium ore host in the North Ordos Basin, occurs as NS-trending units that exhibit distinct depositional hiatuses with both the overlying and underlying formations (Table 1). The Zhiluo Formation can be divided into the Upper Zhiluo and Lower Zhiluo Formations (the latter is further divided into upper and lower submembers) (Table 1). The lower submember of the Lower Zhiluo Formation consists of gray, grayish-white, and grayish-green medium-to-coarse sandstones formed from braided river and braided river delta deposition. The horizon within this submenber, near the underlying Yan'an Formation, which contains abundant carbon debris, pyrites, and carbonate cements, represents the main uranium ore host. The upper submember of the Lower Zhiluo Formation, which consists of mud-sand-mud assemblages of grayish-green medium-to-fine sandstones interrupted by mudstones, from a low-sinuosity meandering depositional environment, is the secondary uranium ore host in this area. The Upper Zhiluo Formation, comprising variegated sandstones interrupted by mudstones, is a fluvial and floodplain depositional system consisting mostly of grayish-green sandstones alternating with red mudstones.

The Lower Jurassic Yan'an Formation, consists of gray sandstones and black coal measures from fluvial-lacustrine and swamp environment deposition (Table 1). Some authors have suggested the white sandstone bed at the top to be an oil or gas-bleached zone (Wu et al., 2015) or to be of paleo-weathering regolithic origin (Jiao et al., 2015; Zhang et al., 2017b).

The area has relatively stable sedimentary formations and only weakly developed regional structures, as manifested by the Hanggin Banner fault zone (including the Bojiang Haizi fault) (Yang et al., 2013, 2015). After analyzing remote sensing images of North Ordos Basin, Liu et al. (2006b) suggested that the area features annular tectonic zones, as manifested by the NW–SE Dongsheng–Shiwanzi fault-uplift zone and the Benhai Aobao–Zhunge'erzhao fault.

In Heishitougou, Hanggin Banner, the Cretaceous sandstones are

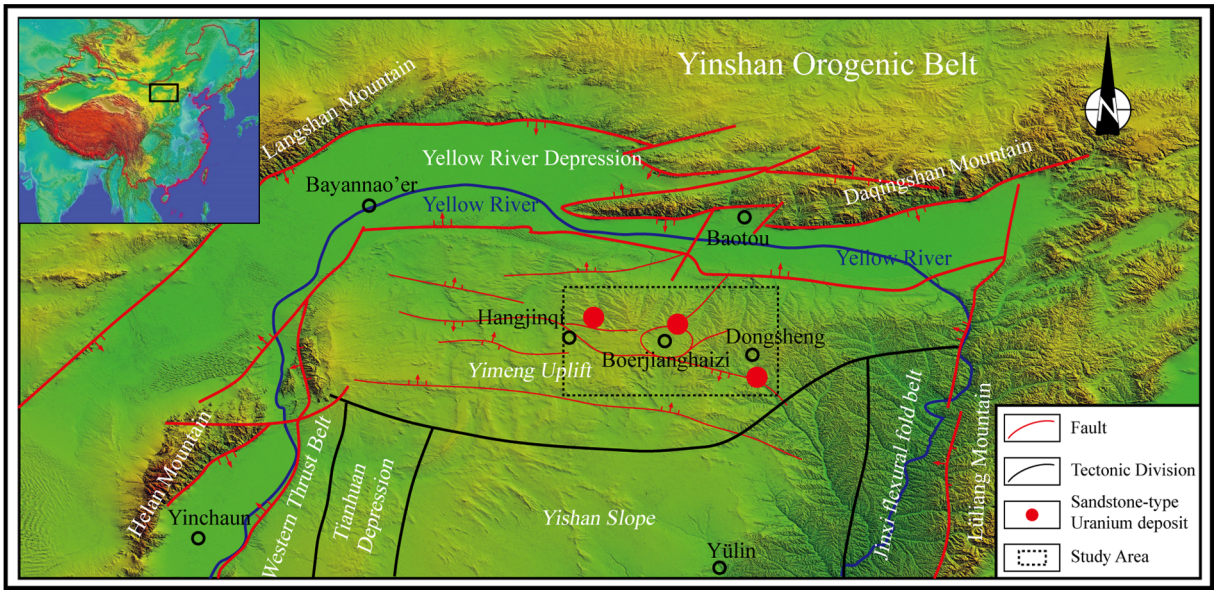

Fig. 1. Digital elevation model tectonic division map of the North Ordos Basin.

Table 1
Composite stratigraphic column of the North Ordos Basin (Modified after Chen et al., 2016, and references therein).

Stratum	Column	Sedimentary makers	Lithology	Sedimentary Enviroment		Pyrite	Uranium	Organics
Cretaceous			Conglomerate, glutenite	Alluvial fan				
Jurassic / Zhiluo Formation / Upper Member		Contains medium or large trough cross-beddings	Brownish-red/grayish-green medium-fine sandstone with thin-layered yellow fine sandstone, thin siltstone layers are observed in the upper part	Channel	meande-ring river	Oxidized lump pyrite		
		Numerous animal burrows are observed in the mudstone, trough cross-beddings are observed in the sandstone	Mudstone, siltstone, mostly containing grayish-green sandy lumps, trough sandstone layers, with the sandstone showing an up-thinning positive rhythm	Floodplain, lacustrine	Arid lake			
		Trough cross -beddings		Channel	High-sinuosity meande-ring river			
		Numerous animal burrows are observed in the mudstone		Lacustrine	Arid lake			
Lower Member / Upper Submember		Contains large cross-beddings, carbon debris and animal burrows are observed in the mudstone	Mostly consists of grayish-green midium fine coarse sandstone, midium-coarse sandstone, with layers of green siltstone and mudstone.	Floodplain	Low-sinuosity meande-ring river	Banded, lumpy, disseminated, colloidal pyrite		
				Channel				
Lower Submember		Animal burrows, carbon debris are seen in the mudstone at the top, large trough cross-beddings are present in the sandstone	Mostly consists of green, grayish-green, light gray or gray medium-coarse sandstone. The sandstone is well sorted, subangular in shape, and loosely consolidated with argillaceous cementation. Calcareous cementation and pyrite cementation are locally observed. Pyrite and carbon debris are widely present in the lower part. Carbonaceous strips are observed in the upper part. In some places, thin coal layers can be detected in the mudstone at the top. The bottom consists of conglomerate and gritstone.	Floodplain	braided river	Banded, lumpy, disseminated, colloidal pyrite	Rich U in medium-coarse sandstone	Carbon debris
				Channel				
Yan'an Formation		Coal Bed	Grayish-black mudstone, siltstone interrupted by sandstone, containing a lot of coalbeds	Fluvial-lacustrine, swamp		Banded, lumpy disseminated, colloidal pyrite	Coal	

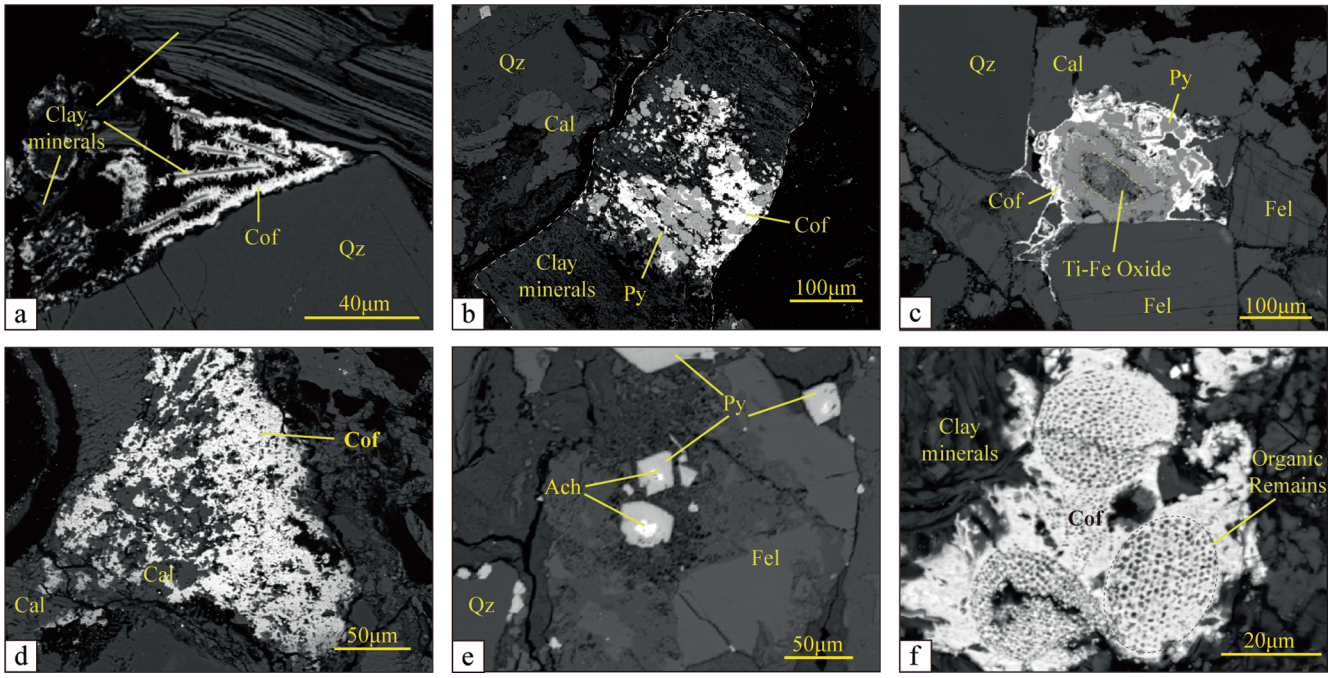

Fig. 2. Major altered characteristics of uranium deposits in North Ordos Basin a-Clay-minerals spatial symbiotic with coffinite; b-Pyrite, coffinite and clay minerals bearing in the altered feldspar; c-Pyrite, coffinite and calcite bearing surrounding the Ti-Fe oxide; d-Calcite spatial symbiotic with coffinite; e-Achavalite coated by pyrite; f-Coffinite bearing surrounded and in the fossils. Ach-Achavalite.

overlain by a basalt bed from the Early Cretaceous with a whole-rock Ar/Ar age of 126 Ma (Zou et al., 2008), which is close to the age of the Zijinshan rocks in the Eastern Ordos Basin (137–130 Ma) (Yang et al., 2009a). This suggests the occurrence of a tectonic–magmatic–thermal event in the area in the Early Cretaceous (Zou et al., 2008).

In the North Ordos basin, uranium ore-bodies were mainly hosted in the gray sandstone of the Lower Zhiluo Formation. Compared with the uranium deposits in Yili basin and Qianjiadian area of Songliao basin, its ore-body shape shows the tabular instead of roll-type (Jin et al, 2019 and references therein). The occurrence of uranium minerals is coffinite with a few of pitchblende (Bonnetti et al., 2015, 2017; Dai et al., 2015; Akhtara, et al., 2017). The concentration of uranium minerals had the spatial symbiotic relationship with organic materials, calcite, pyrite, reducing bacteria, oil–gas, and so on (Cai et al., 2007; Fan et al., 2007; Feng et al., 2017). In the study area, the major low-temperature alteration characteristics related to the uranium mineralization, are clay mineralization (such as smectite, chlorite, kaolinite, illite, and so on) and sericitization of K-feldspar (Akhtara, et al., 2017; Fan et al., 2007; Zhao et al., 2018c) (Fig. 2-a&b). Clay minerals commonly exist as cementing clasitc grains, altering of mica or feldspar minerals, surrounding the clastic grains in form of thin-film, or spreading into the matrix as acicular crystals, all of which can be found to have the spatial relationship with coffinites. Some authors thought that uranium mineralization was the result of mixing of shallow meteoric water and deep-source fluid from the crust (Li et al., 2007; Xue et al., 2010). Although the formation of pyrites is multistage, the pyrites having the spatial symbiotic relationship with uranium minerals, are in colloidal or framboidal form (Fig. 2-b&c). The Ti-Fe oxides often spread in the ore-bearing layers. Influenced by ore-forming fluid, most of them were altered, kept their original shape and surrounded by pyrites and coffinites (Fig. 2-c). Besides, achavalite commonly coexisted with pyrites and coffinites in the Lower Zhiluo Formation (Fig. 2-f).

3. Sampling and methods

The samples of Zhiluo Formation were collected from more than 10 drill cores in the Nalinggou, Tanrangaole and Daying uranium deposits in the North Ordos Basin. All are located in the uranium ore-body bearing layers in the Lower Zhiluo Formation. The samples of Yan'an Formation came from the Shenshangou outcrop located at the southeast of Dongsheng. The thin-sections were made in the Yu'neng Geological Laboratory in Langfang, Hebei, China.

The micro-photos were taken under the Leica DM2700 M. Electron Probe Microanalyzer (EMPA-1600 of Shimaduz Corporation, Japan) were used to analysis the microscopic characteristics of minerals in the Geological Laboratory of Tianjin Center, China Geological Survey. The work conditions are as follows: 15 kV of Acceleration voltage, 20 nA–100 nA of current, 1 μm–5 μm of beam, 20–60 s of peak computing time, 40° of exist angle. The ZAF method is used to revise results data. The standard samples are SPI sulfide and Gold-Silver sample. The SEM analysis was used of the SS550 of Shimaduz Corporation, Japan. The chemical contents analysis of uranium minerals were conducted in the Analytical Laboratory CNNC Beijing Research Institute of Uranium Geology by using HEOL's JXA-8100 electron microprobe. The S isotopic analysis, Trace elements and REE analysis were undertaken in the Analytical Laboratory CNNC Beijing Research Institute of Uranium Geology.

4. Morphology of the pyrite and its relationship with other altered minerals

Pyrites of varying morphologies are widespread throughout the Zhiluo Formation of the uranium orefield in the North Ordos Basin (Fig. 3), and have been found to have close spatial correlations with the uranium ore distribution (Liu, 2011; Chen et al., 2016). In this study, detailed analyses of the morphology and composition of the pyrites in the orefield are conducted through hand specimen analysis, microscopy, electron probe microanalysis (EPMA), and scanning electron microscopy (SEM). Their paragenesis with other altered minerals is observed and further discussed.

4.1. Macro- and microscopic characteristics of the pyrites

Field work and drill core observations reveal that the pyrites formed

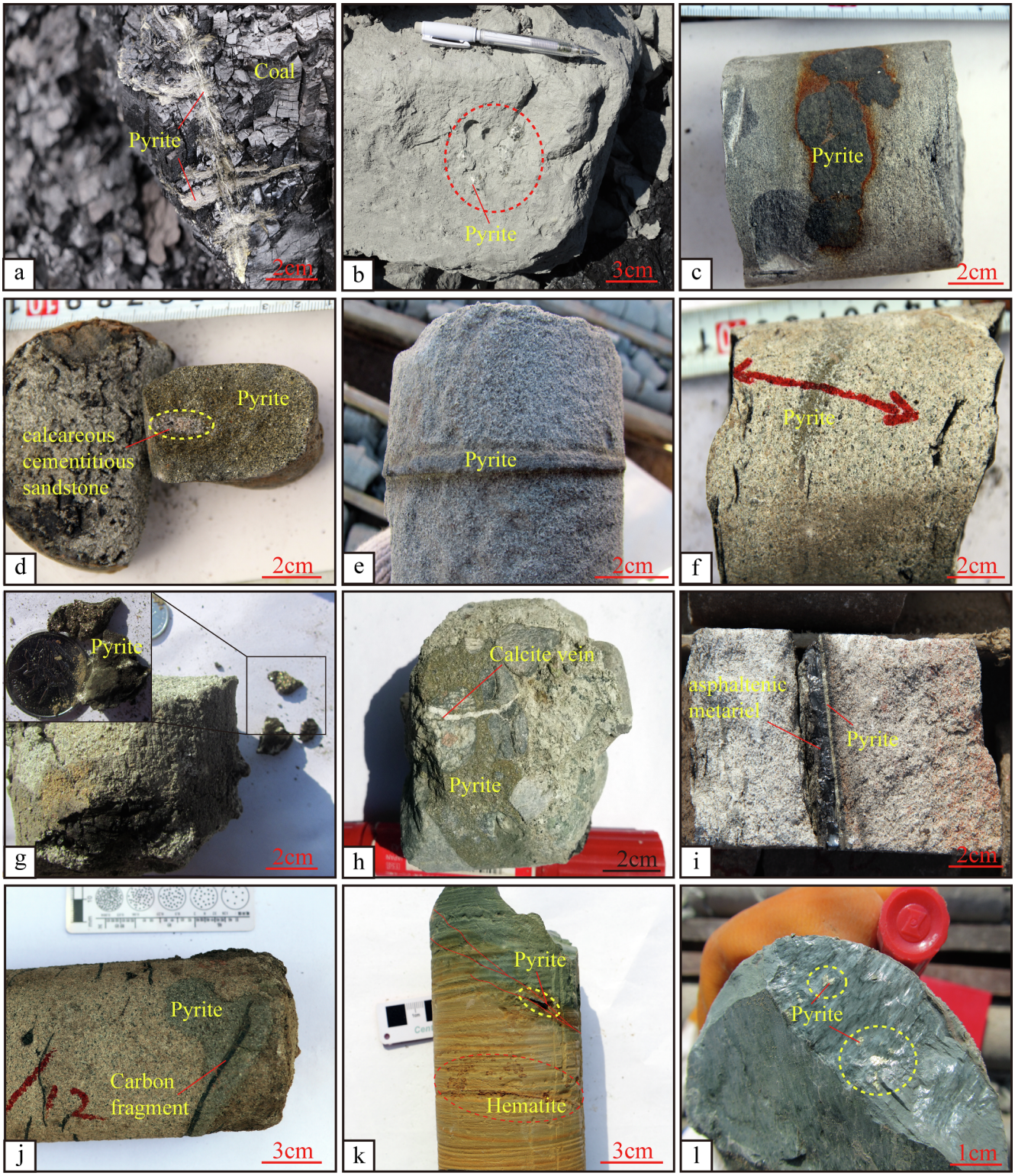

Fig. 3. Morphology of the pyrites in Yan'an and Zhiluo Formations, North Ordos Basin a- Two generations of veinlet pyrites present in the coalbed fissures, Yan'an Formation; b- Spherical pyrites in the gray sandstones, Yan'an Formation; c- Oxidized brown hematitic zones are observed on the periphery of the lumpy pyrites in the gray sandstones, Zhiluo Formation; d- Sandstones cemented by red carbonates within the pyrite lumps, Zhiluo Formation; e- Platy pyrites in the gray sandstones, Zhiluo Formation; f- Disseminated pyrite grains with metallic luster in the gray sandstones, Zhiluo Formation, which were subsequently cemented by carbonates; g- Star-like pyrites in the gray sandstones, Zhiluo Formation; h- Pyrite cementation in the conglomerates at the bottom of the Zhiluo Formation, which were subsequently cemented by carbonates; i- Banded pyrites bordering the carbon debris or bituminous organisms inside the grayish-white sandstones, Zhiluo Formation; j- Pyrite-carbon debris aggregates in the grayish-white sandstones, Zhiluo Formation which are cemented by carbonates; k- Brown oxidized/hematized pyrites and fractures in the brown sandstones, Zhiluo Formation, with the upper parts of the fractures appearing in green; l- Sheet-like pyrites on the slickenlined fault surface in the green argillaceous siltstones, Zhiluo Formation. (For interpretation of the references to color in this figure legend, the reader is referred to the web version of this article.)

either in gray or grayish-green sandstones and mudstones, or in coalbeds or other highly reducing environments. Brown oxidation stains can be detected around some of the pyrite nodules.

The Yan'an Formation is mainly composed of coalbeds interrupted by gray sandstones or siltstones, which indicates a highly reducing environment. The pyrites in the coalbeds, which occur in fissures in banded form, originate from at least two periods (Fig. 3-a). The pyrites in the Yan'an sandstones, however, occur as spheres of pyrite-cemented sandstones, which are mostly a few centimeters in diameter (Fig. 3-b). Cubic crystals with good metallic luster are found on the surface of some of the pyrite spheres.

In the Zhiluo Formation, pyrites are mostly found in the gray and green sandstones of the lower member. Macroscopically, they occur in lumpy (or subspherical), banded (or platy), disseminated, star-like, or sheet-like form (Fig. 3). Pyrite-cemented sandstone inside the lumpy pyrites, which is the typical morphology of the pyrites in this formation, occurs along the same horizon as carbon debris. Some of these pyrites are also observed to envelop carbon debris (Fig. 3-j). In the conglomerates at the bottom of the Zhiluo Formation, pyrites have cemented gravels and early carbonate cements, and are themselves cemented by younger carbonate cements (Fig. 3-h). Banded pyrites mostly occur along the edges of laminations and carbon debris. In drill cores, they mostly appear as thin sheets of about 2–10 mm thick, parallel to the laminations (Fig. 3-e&i). Disseminated pyrites spread outwards from banded or lumpy pyrites (Fig. 3-f). Star-like pyrites typically exist in carbon debris or in black mudstones or other highly reducing locations (Fig. 3-d). In addition, oxidized pyrite remnants exist in the oxidized brownish-yellow-coloured sandstones. On the outcrop, some faults are observed inside the Zhiluo Formation, while based on the observation of drill cores, many fractures are obtained (Fig. 3-k). Around the small-scale fault planes, the color of the sandstones is green and on their surfaces, sheet-like pyrites with good metallic luster are present (Fig. 3-k&l).

Based on the microscopic analysis, the sandstones are commonly cemented by pyrites and carbonates in the ore-bearing segments (Fig. 4). Detritus in the sandstone in the ore-bearing segments mainly includes feldspar, quartz, lithic fragments (rock debris), and mica minerals, all of which occur in angular form and indicate proximal deposition (Fig. 4-a). Locally, the detrital grains are coated by a clay mineral overgrowth on the surface (Fig. 4-b). Some authors have suggested that this overgrowth served as an important adhesive agent for the subsequent enrichment of uranium minerals (Li et al., 2007; Xing et al., 2008; Xiang et al., 2006a). As commonly seen in the ore-bearing segments, carbonates either cement detrital grains or fill fissure in the earlier carbon debris, and comprise either micritic or sparry calcites. Pyrites mainly occur in colloidal or framboidal form, while their exact formation period cannot be identified under the microscope. The major existing forms of pyrites are (1) cementing detrital grains, (2) developing on detrital grains, and (3) developing in carbon debris fissures. Locally, it is also observed that pyrites fill the cleavages of altered mica minerals and to occur surrounding altered Ti-Fe oxides. As uranium minerals are difficult to detect under a microscope, the relationships between the pyrites, calcites, and other altered minerals, and the uranium mineralization are difficultly determined satisfactorily by using optical microscope.

To further examine the micromorphology of the pyrites and their spatial relationships with the dominant uranium minerals (coffinite and pitchblende) and other minerals, EPMA was used to analyze the ore-bearing sandstones. With this higher magnification, the microscopic characteristics of the pyrites are found to be even more complex. The observed forms of pyrites are (1) as detrital grains or inside detrital grains, (2) as idiomorphic grains, (3) in colloidal or framboidal form, (4) inside mica minerals, (5) in banded or petaloid form, and (6) in other forms related to biological cells or microorganisms. (Fig. 5). In EPMA back-scattered electron images, microscopically observable lumpy pyrites mainly appear in colloidal form. In most cases, the pyrites exist in colloidal form by cementing detritus grains with coffinite hosted on the margins (Fig. 5-d). Some grains also exist in framboidal form and inside the cleavages of mica minerals (Fig. 5-e and f). Some of the framboidal pyrites are cemented by younger colloidal pyrites, or have coffinite within the framboids. The banded pyrites only are observed to develop in the fissures or on the margins of carbon debris, and to exhibit close relationships with organic matter (Fig. 5-g). In a few samples, it is also observed that pyrites spread as separate detrital grains with regular morphology or are broken into pieces (Fig. 5-a). Given that some of the pyrites also exist within granitic or metamorphic detrital grains (Fig. 5-b), a small amount of the pyrites ought to originate during sedimentation or from the underlying formations and have been preserved in a constant reducing environment. The annular texture found in the petaloid pyrite signifies different periods of growth (Fig. 5-h). Previous works have noted the ubiquitous presence of plant fossils and microorganisms in the Zhiluo Formation (Chen et al., 2016; Hou et al., 2016; Sun et al., 2017). In this study, some pyrites are found to occur inside the detrital cells of plant fossils or to have enveloped minute carbonized microorganisms (Fig. 5-i).

The EPMA study results reveal a close spatial paragenesis of the pyrites with uranium minerals, as indicated by the occurrence of coffinite around the pyrites with no obvious mineralization within the pyrites (See Fig. 5-g and Fig. 8-a in the Section 4.3.1).

4.2. SEM profiles of the pyrites and uranium minerals

Based on SEM imaging, the micromorphology and spatial configuration of different types of pyrites relative to uranium minerals are shown in Fig. 6. SEM images reveal that the framboidal pyrites consist of many neo-crystal grains, most of which exhibit to be cubic or spherical (Kalatha and Economou-Eliopoulos, 2015; Zhou et al., 2017) (Fig. 6-a). The uranium minerals have cemented pyrite spherical grain aggregates (Fig. 6-c), while the colloidal pyrites display flat crystal habits inside and come into contact with the uranium minerals on the outside grain margins in irregular form (Fig. 6-d). The uranium minerals mainly exist as minute plates, stubs, or needles, with most of the sheet-like uranium minerals being smaller than 2 μm in size. Most of the stub- or needle-like uranium grains are smaller than 1 μm. As discovered by previous authors when examining the coal combustion process, the larger the specific surface area and porosity of the pyrite grains, the stronger is their degree of reduction (Xiang, 2009). On these grounds, since they have a larger specific surface area, it is suggested that framboidal pyrites are more conducive to the reduction–precipitation of the uranium minerals than their colloidal counterparts.

4.3. Spatial relationships of the pyrites with other altered minerals

Mineral alterations present in the sandstone-type uranium deposits in the North Ordos Basin, China include pyritization, as well as clay mineralization and carbonatization. Depending on the lithological stage (diagenetic or metallogenic), the development order and main development stage of these alterations vary, as do their relationships with the enrichment of uranium minerals. In this study, EPMA is used to examine the spatial relationships and development order of the pyrites relative to carbonates, achavalite (FeSe), Ti-Fe oxides, and coffinite/pitchblende.

4.3.1. Spatial relationships of pyrite with carbonates

Pyritization and carbonatization represent the most typical alterations in and around the sandstone-type uranium deposits in the North Ordos Basin, and are also closely associated with uranium mineralization (Li et al., 2008; Chen et al., 2016; Feng et al., 2016; Zhang et al., 2017a). The microscope analyses revealed the following relationships between the pyrites and carbonates (Fig. 7).

Some colloidal or dyke-type pyrites formed later than the

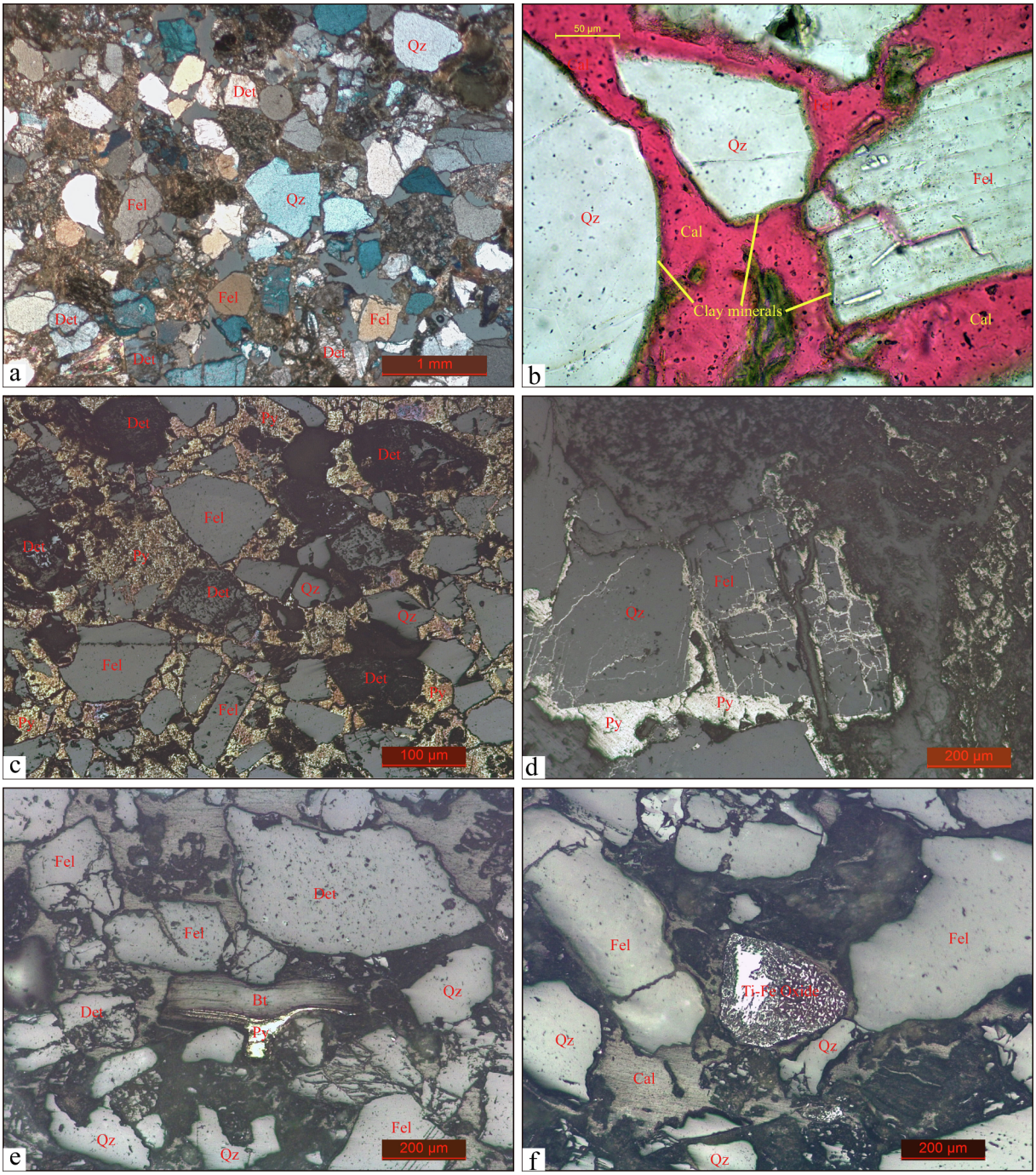

Fig. 4. Photomicrographs of ore-bearing sandstones a-Zhiluo sandstones, with detrital grains occurring in angular form and mud cementation or calcareous cementation (transmission light); b-Carbonate-cemented sandstones with clay minerals occurring on the surfaces of the detrital grains (transmission light); c- Pyrite-cemented sandstones (reflected light); d-Pyrite-cemented sandstones with pyrites occurring in the fractures of detrital grains (reflected light); e-Pyrites developing along the cleavages of mica minerals (reflected light); f- Altered Ti-Fe oxides. Det: detrital grains; Fel: feldspar; Qz: quartz; Bt: altered biotite; Cal: calcite; Py: pyrite; Ti-Fe Oxide: Titanium-iron oxide;

carbonates (Figs. 7-a&b and 8-a). Carbonates exist in the Zhiluo Formation in three forms: micritic calcites, sparry calcite detritus, and colloidal sparry calcites, with the latter being closely associated with mineralization. Some of the pyrites are found to have cemented the detrital grains of calcites. The calcite detritus is obviously angular in shape, which suggests that the grains are the result of near-source transport or in-situ fragmentation of early colloidal calcites. Then, they were subsequently cemented by pyrites such that their original morphology is preserved.

Some the colloidal pyrites and uranium mineralization formed contemporaneously with the some carbonates (Fig. 7-c&d). The pyrites, calcites, and coffinites comprise irregular harbors by interweaving with each other. Locally, irregular pyrites occur inside calcites, with coffinites occurring between the pyrites and calcites. These findings confirm that these pyrites developed contemporaneously with the carbonates, although the carbonates may have crystallized a little later than the pyrites and coffinites. The pyrites and carbonates formed during the uranium metallogenic stage, and are therefore primary subjects for studying the ore-forming fluids.

Some framboidal, idiomorphic crystal, and colloidal pyrites formed

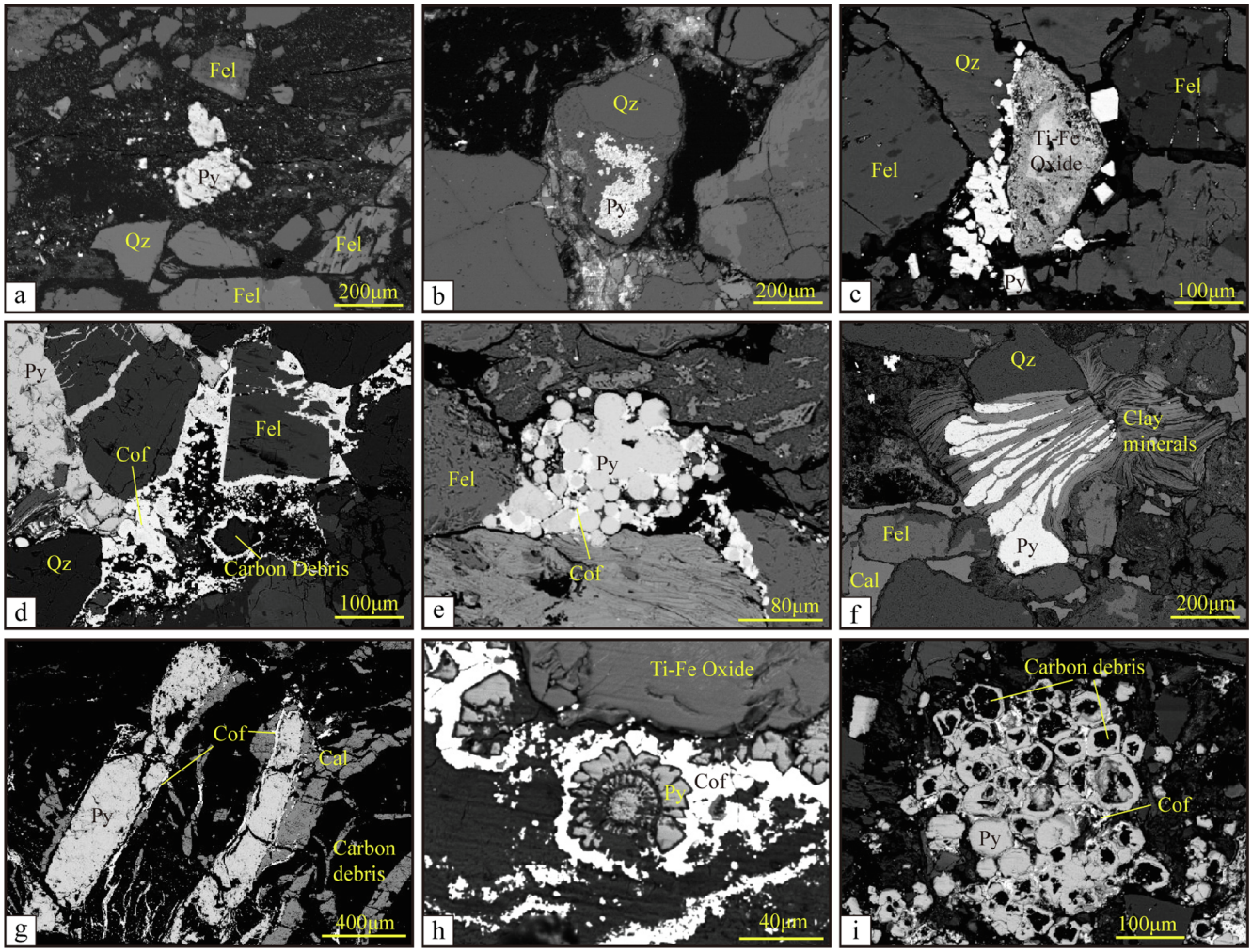

Fig. 5. Microscopic characteristics of the pyrites a- Pyrites existing as separate detrital grains; b- Pyrites occurring inside detrital grains; c- Subhedral pyrites with good crystal morphology; d- Pyrite cementing detrital grains; e- Framboidal pyrites; f- Pyrites in mica cleavages; g- Banded pyrite-calcite; h- Petaloid pyrites surrounded by coffinite; i- Organism-related pyrites mantling carbon debris. Fel- Feldspar; Qz- Quartz; Py- Pyrite; Cal- Calcite; Cof-Coffinite.

earlier than the carbonates (Figs. 7-e&f and 8-b). Coffinites and clay minerals developed on the periphery of the idiomorphic pyrites, which are cemented by younger calcites, and calcite veinlets developed along the pyrite fissures (Fig. 7-f).

The spatial relationships of the pyrites with carbonates, therefore, indicate the order of the two most important alterations during the formation of the sandstone-type uranium deposits. It further shows the chronological relationships of the different periods of pyrites or carbonates with uranium enrichment. This is very significant for determining the alterations that occurred during the metallogenic stage.

To further explain the spatial relationships between the pyrites and carbonates, we performed EPMA element-area scanning to map the spatial distributions of Ca, Fe, S, U, K, and Mg. Parts of the samples consist of veins of pyrites interwoven with carbon debris and calcite fissures, with uranium mineralization at the intersections. In the chemical maps, carbonates, pyrites, and coffinites are in sharp contact, which indicates that there is no obvious migration replacement between the minerals by Ca, Fe, U, or S. The genetic sequence of the three minerals is as follows: carbonates boring in the organic debris > dyke-type pyrites > coffinites. As there is a lot of carbon debris on the periphery, it cannot be determined here whether there is a direct redox relationship between the pyrites and coffinites or not. The remaining sample consisted of carbonate-enveloped pyrites, coffinites, K-feldspars, and clay minerals. Grains of K-feldspar and pyrite comprise the core, accompanied by small amounts of clay minerals and coffinites on the periphery. In this sample, the core appears to consist of K-feldspar grains surrounded by clay minerals and star-like pyrites. Some of the pyrites have very good idiomorphic crystals, which are also accompanied by a small amount of clay minerals. Coffinite occurs around K-feldspars, pyrites, and clay minerals. All these minerals have eventually been cemented by carbonates. This indicates the genetic order of the main altered minerals, as follows: idiomorphic crystal pyrites > coffinites > colloidal or dyke-type carbonates. The results demonstrate that the pyritization and carbonatization processes had multiple stages. In addition, the distribution of Mg element and disappear of Fe element also indicates the presence of smectite membrane coating on the surface of the K-feldspar.

4.3.2. Spatial relationships of pyrite and achavalite

Se, as a dispersed element, is rarely enriched into a deposit in the natural world, and individual Se minerals are rarely found (Tu and Gao, 2003). As S and Se have very similar geochemical properties, including ionic radius (S^{2-}: 0.184 nm, Se^{2-}: 0.191 nm), lattice energy coefficient (S^{2-}: 1.15, Se^{2-}: 1.10), and ionic potential (S^{2-}: −1.09ev, Se^{2-}: −1.05 eV), Se mostly exists in pyrites in isomorphic form (Liu et al., 2001), substituting for S element. In the sandstone-type uranium ore-bearing segments of the North Ordos Basin, pyrites (FeS_2) are frequently observed to be co-genetic with achavalites (FeSe) (Fig. 2-e), and some pyrite samples also contain some Se. The EPMA area scanning maps indicate that the achavalites are enveloped by pyrites or contain S

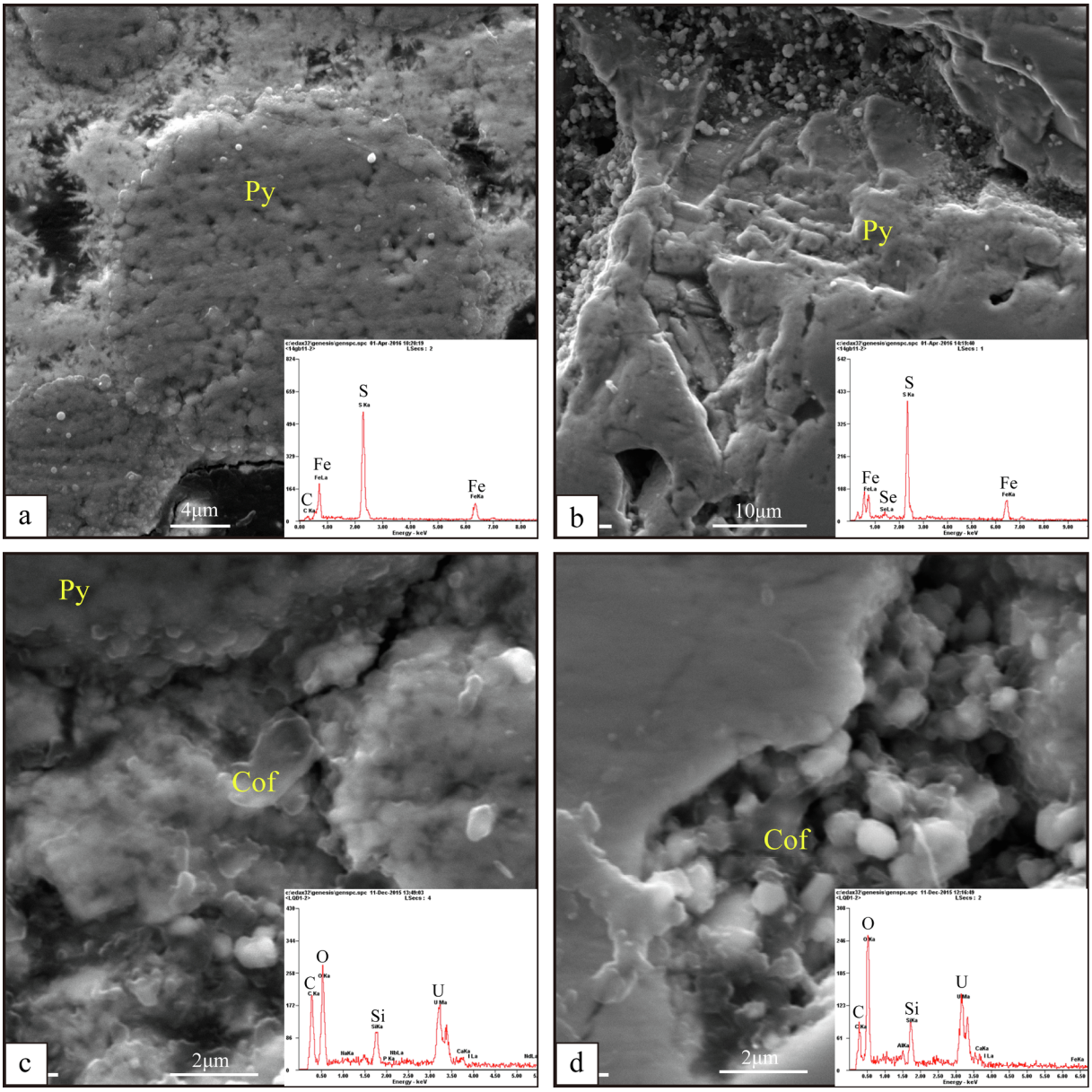

Fig. 6. SEM images showing the morphologies and EDS mineral chemistries of the pyrites and coffinites.

(Fig. 9-a), and it is found that no Se element in the surrounding pyrites. Furthermore, achavalite growth zones are present in some pyrites, which have been subsequently enveloped by Se-free pyrites (Fig. 9-c). Coffinite is present either on the periphery of pyrite–achavalite aggregates or between the achavalite and pyrite grains. These pieces of evidence suggest that there is some historical Se enrichment in the Zhiluo Formation. Spatial distribution analysis revealed the paragenetic order is as follows: achavalite > pyrite > coffinite.

4.3.3. Spatial relationship of the pyrite with Ti-Fe oxides

Numerous detrital Ti-Fe oxides have been found in the sandstone-type uranium deposits of the North Ordos Basin (Figs. 2-c, 10). However, in the ore beds, these oxides have been altered and degraded into Ti oxides or brannerites ($(U,Ca)(Fe,Ti)_2O_6$). EPMA element-area scanning mapped the spatial relationships and evolutionary sequence of the Ti-Fe oxides, pyrites, and uranium minerals and provided evidence concerning the progress of uranium mineralization. The original Ti-Fe oxides existed as detrital grains of ilmenites. Later, affected by diagenetic fluidization, the Fe in the Ti-Fe oxides precipitated out of the Ti-Fe oxides and was ultimately replaced by Ca, U, and V (Fig. 10). The precipitated Fe elements combined with the S elements in the fluids to form pyrites on the periphery of the Ti-Fe oxides. This explains why these elements exist in zonal form, with Ti and Fe at the core; Ti, Ca, and U located away from the core; and S and Fe on the periphery of the grains. Although coffinites are mostly found to occur around the aggregates of Ti-Fe oxides and pyrites, many are also present on the edges of the matrixes or other detrital grains. In addition, many micritic calcite and V compounds are hosted in these matrixes. V element is mostly found in the matrixes, although it is also locally observed as V-oxide, an irregular mineral. When investigating the V element distribution in the Grands U–V–Cu deposit, previous authors determined that, having been affected by subsequent organic fluids during the metallogenic stage, V element had precipitated out of Ti-Fe oxides and was enriched in the nearby matrixes (Webster, 1983; Turner-Peterson, 1985). Other authors have attributed V enrichment to the wide presence of V-rich chlorites during the metallogenetic stage (Fishman et al., 1985), and assumed that Vand U precipitated synchronously by the interaction of the two fluids (McLemore, 2010). In this study, the

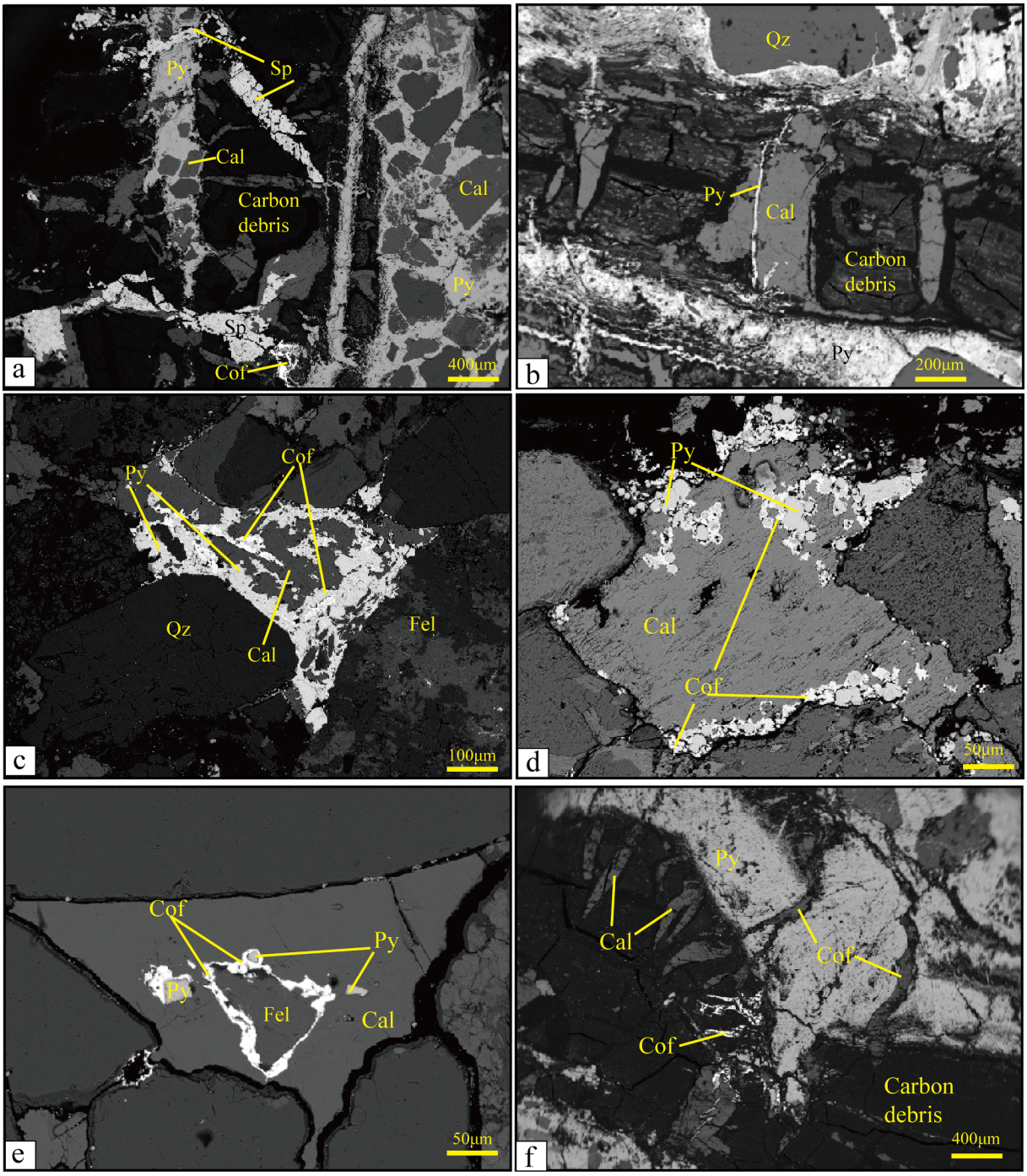

Fig. 7. Spatial distribution of pyrites relative to the carbonates (calcites) and coffinites a-Pyrite-cemented brecciated calcites; b- Pyrites occurring in veinlet form along calcite fissures; c- Pyrites interwoven with calcites and coffinites in irregular form; d- Pyrites and coffinites occurring inside and on the edges of calcites; e- Calcite-enveloped pyrites, coffinites and K-feldspars; f- Calcites occurring in veinlet form along pyrite fissures. Sp- Sphalerite; others see Fig. 4.

widespread V element in the originally deposited matrixes, under the action of reducing fluids, formed irregular V oxides which were subsequently surrounded by younger uranium minerals. Furthermore, the altered Ti-Fe oxides contain abundant V, whereas none is found in the younger pyrites due to Fe precipitation. During fluidization, the pyrites formed earlier than the V-oxide.

5. Geochemistry of the pyrites

By in-situ EPMA composition analysis, whole-rock trace element, including trace elements, and S isotope geochemistry of the pyrites was determined for the ore-bearing segments. The enrichment of related elements in the pyrites and achavalites were further examined, and the ore-bearing sandstones and mudstones were also compared with the pyrite-bearing sandstones with respect to their mineral chemistries. The implications of the S isotope values in the pyrites with respect to their genesis are discussed.

5.1. Mineral composition

In view of the frequent replacement of S by Se, after the in-situ EPMA analysis of the pyrites and achavalites, the compositional

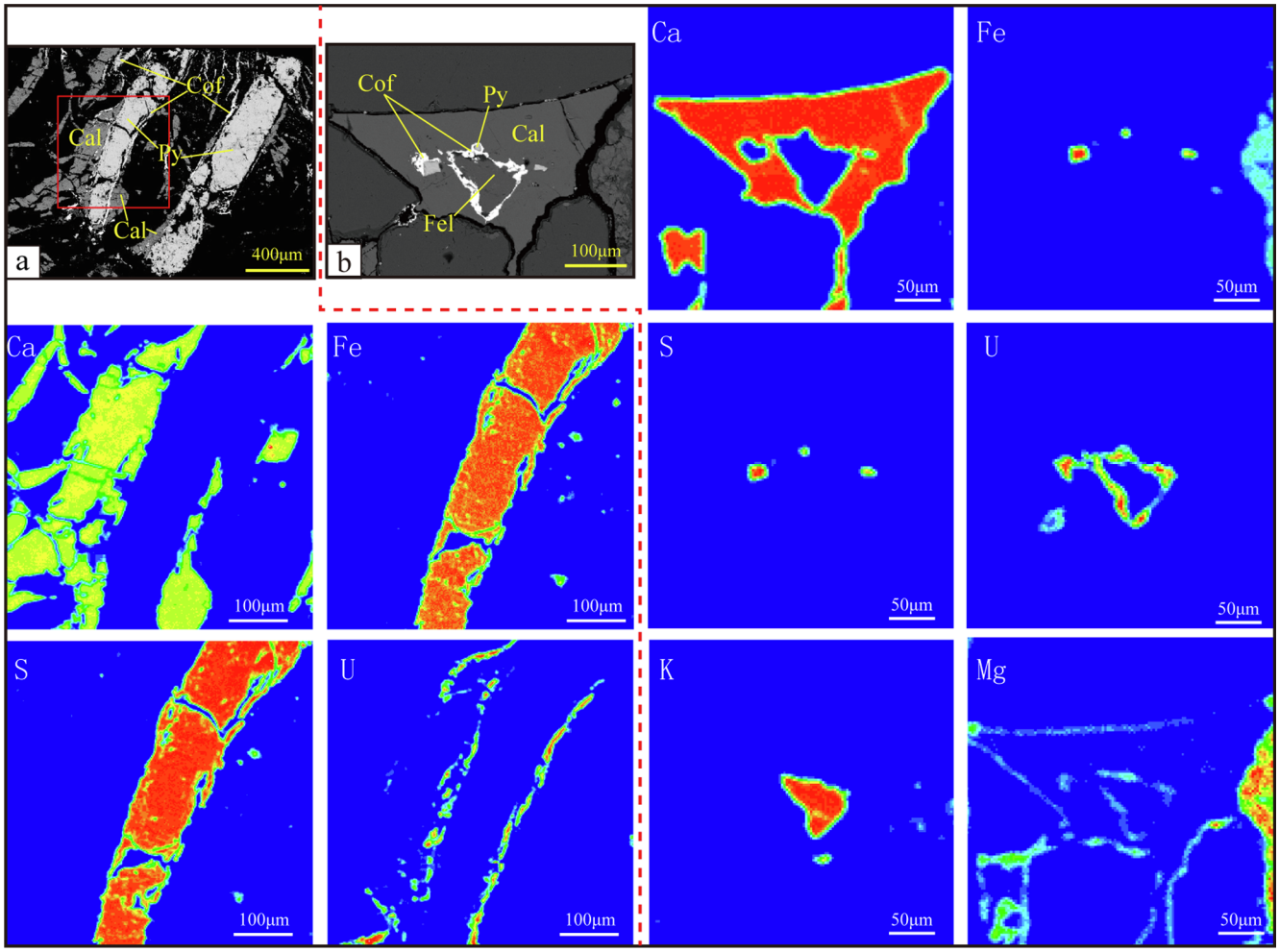

Fig. 8. Spatial relationships and mineral chemical information of the carbonates, pyrites, and uranium minerals, with the EDS area scans of relevant elements (Ca, Fe, S, U, K and Mg) (a, see Fig. 4-g; b, see Fig. 6-e).

differences between these two minerals, and their interactions with related elements were investigated (Table. 2). The S and Se in the two minerals are linearly correlated in terms of percentage (Fig. 11). The As contents are remarkably different in the pyrites and achavalites, being less than 0.1% in achavalite but ranging from 0.1 to 0.7% in pyrite. The Ti contents are the same in the two minerals: less than 0.04% for both. The U content is less than 0.05% in the achavalites but somewhat higher in the pyrites i.e., less than 0.2% in most cases, but reaching as high as 0.7%. This indicates that, during the formation of the sandstone-type uranium deposits, the pyrites formed were richer in U than the achavalites, which supports the previous observation that the achavalites developed earlier than the pyrites, or the timing of the pyrite development was in a period closer to the precipitation of U.

5.2. S isotopes, trace Elements, and REEs

In the natural world, mantle sulfur has a $\delta^{34}S‰$ of 0 ± 3‰; in modern sea water, S has a $\delta^{34}S‰$ of 20‰; in terrestrial depositional rocks, reduced S has a wider range (Rollinson, 1993; Liu et al., 2011). The fractionation of S isotopes in sedimentary rocks is closely associated with the generation of sulfides through sulfate-reducing bacterial processes; the ^{32}S enrichment level in the H_2S produced by the reduction of sulfate is dependent on the concentration of the sulfate and the intensity of the reduction process (Zheng and Chen, 2000; Seal, 2006).

The S isotope analyses of the pyrites in the ore-bearing segments of the Zhiluo Formation and the nearby grayish-green and grayish-white sandstones in the Nalinggou uranium orefield revealed a very wide $\delta^{34}S‰$ range (−7.3‰–37.2‰), although it is mostly on the order of −30‰ indicating a dominance of significantly negative values (Fig. 12). According to the criteria provided by Rollinson (1993), the $\delta^{34}S‰$ distribution of the Nalinggou uranium orefield indicates a biogenic and mixed organic origin for the S isotopes there. Other studies have suggested that the considerable number of negative $\delta^{34}S‰$ values should be proof that the sulfur has a mix of organic sources, including coalbed methane and oil gas (Wu et al., 2006). Through the $\delta^{34}S‰$ analysis of the S isotopes in the Jurassic coalbeds and carbon debris, the crude oils from the Yan'an and Yanchang Formations, and the Upper Paleozoic coal-measure source rocks in the uranium deposits of the North Ordos Basin, Wu et al. (2016) concluded that the S in the pyrite of the Zhiluo Formation comes from the natural gases produced by the deep Upper Paleozoic coal-measure source rocks. These reducing gases were extensively dissipated northward from the basin center along deep, large faults. In the Zhiluo Formation, the mass of H_2S, either released through decomposition under sulfate-reducing bacterial processes or contained in the formation itself, participated in the formation of pyrites there. In addition, the wide $\delta^{34}S‰$ variation also takes into account the sedimentary origin of some of the pyrites, such as the detrital pyrites in the Yan'an and other stratum, and the primary pyrites in the Zhiluo Formation (Fig. 5-a).

A trace elements analysis on the ore-bearing sandstones, pyrite-bearing sandstones, and ore-bearing mudstones in North Ordos Basin, suggests that the trace elements geochemistry of the mudstones, which have been less influenced by fluidization due to their limited permeability, represent the trace elements distribution during the primary

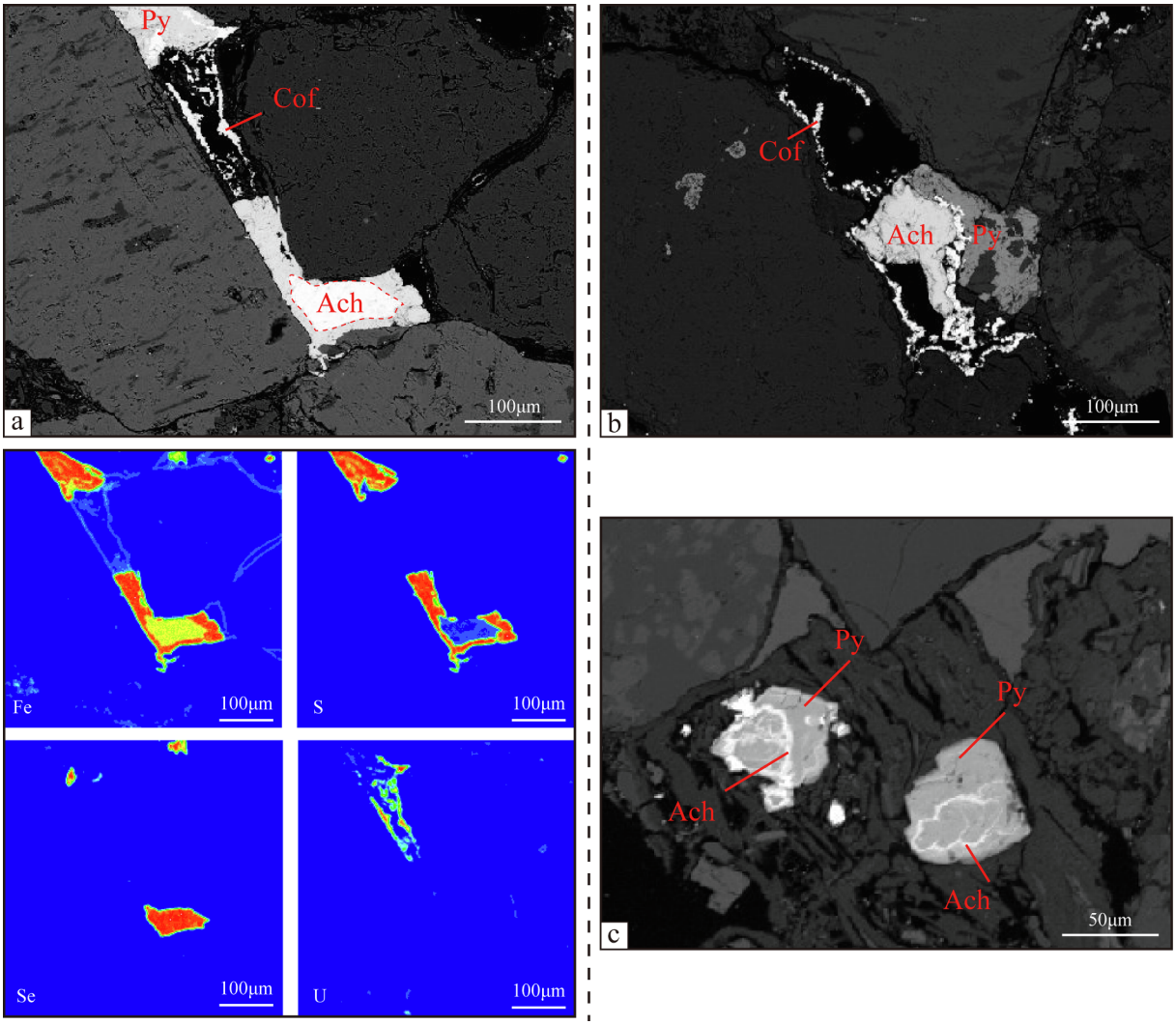

Fig. 9. Spatial relationships and mineral chemical information of the pyrites, achavalites, and coffinites, with the EDS area scans of relevant elements (Fe, S, Se, and U).

sedimentation (Fig. 13). Based on the Chinese sedimentary rock standard value, compared with the mudstones, the ore-bearing sandstones have trace elements distributions more similar to those of the pyrite-bearing sandstones: they are typically rich in U, Mo, and Ba, and poor in Cs, Th, and Bi (Fig. 13). It further confirms that subsequent fluidization is responsible for the U enrichment in the sandstones.

As the REEs are insoluble and less concentrated in the water, the most significant factor affecting the REE contents of sandstone is the provenance (Fleet, 1984; Mclennan, 1989; Ling et al, 2006). In this work, the REEs of sandstones with ore bodies, sandstones with pyrites, and mudstones surrounding ore-body bearing layers are analyzed (Fig. 13). The REE patterns show that the light REEs are enriched and the heavy REEs are depleted. The light REEs' pattern has a right trend, while the heavy REEs' patterns are almost flat. It states that there is a great differentiation between the light and heavy REEs. The patterns of REEs are almost same among different layers, indicating that they have the unified provenance, sedimentary and tectonic geological background. Compared with the REEs of sandstones, δEu of mudstones shows a light negative anomaly. Besides, the REE total amounts of sandstones are less than that of mudstones. It indicates that the ore-forming fluid have affected the spread of REEs in sandstones. Because of low permeability, mudstones are less influenced by ore-forming fluid, which can be recognized as the geological background for REEs' study.

6. Occurrence of uranium minerals

Most previous studies have considered coffinite to be the principal uranium mineral in the sandstone-type uranium deposits in the North Ordos Basin. The presence of pitchblende has been mentioned in previous studies, however none provided direct evidence (Yang et al., 2009b; Liu et al., 2013; Ma et al., 2013; Chen et al., 2017b). In the EPMA electron backscatter diffraction (EBSD) images, bright, round dots can be seen amid the more massive coffinite. An in-situ compositional analysis revealed a SiO_2 content of less than 5% (Table 3, red bold italic data). Given the influence on the EPMA by SiO_2 from the surrounding coffinites, it is highly probable that these dots represent the presence of minor amounts of pitchblende.

Upon examining the EBSD images, the coffinites, as the typical uranium mineral in these uranium deposits, are mostly found inside metamorphic or granitic detrital grains, on the periphery of clay minerals or various pyrites, in carbon debris fissures, or inside paleontological fossils (Figs. 5 and 7). While, pitchblende often exist in the coffinite grains (Fig. 14). Together, these locations reflect the genetic relations of the uranium minerals in the sandstone. The presence of uranium minerals in metamorphic or granitic detrital minerals suggests original pre-enrichment from the provenance during the sedimentary diagenesis, and the preservation of uranium minerals are kept well from alteration by the subsequent fluidization. Enrichment of uranium

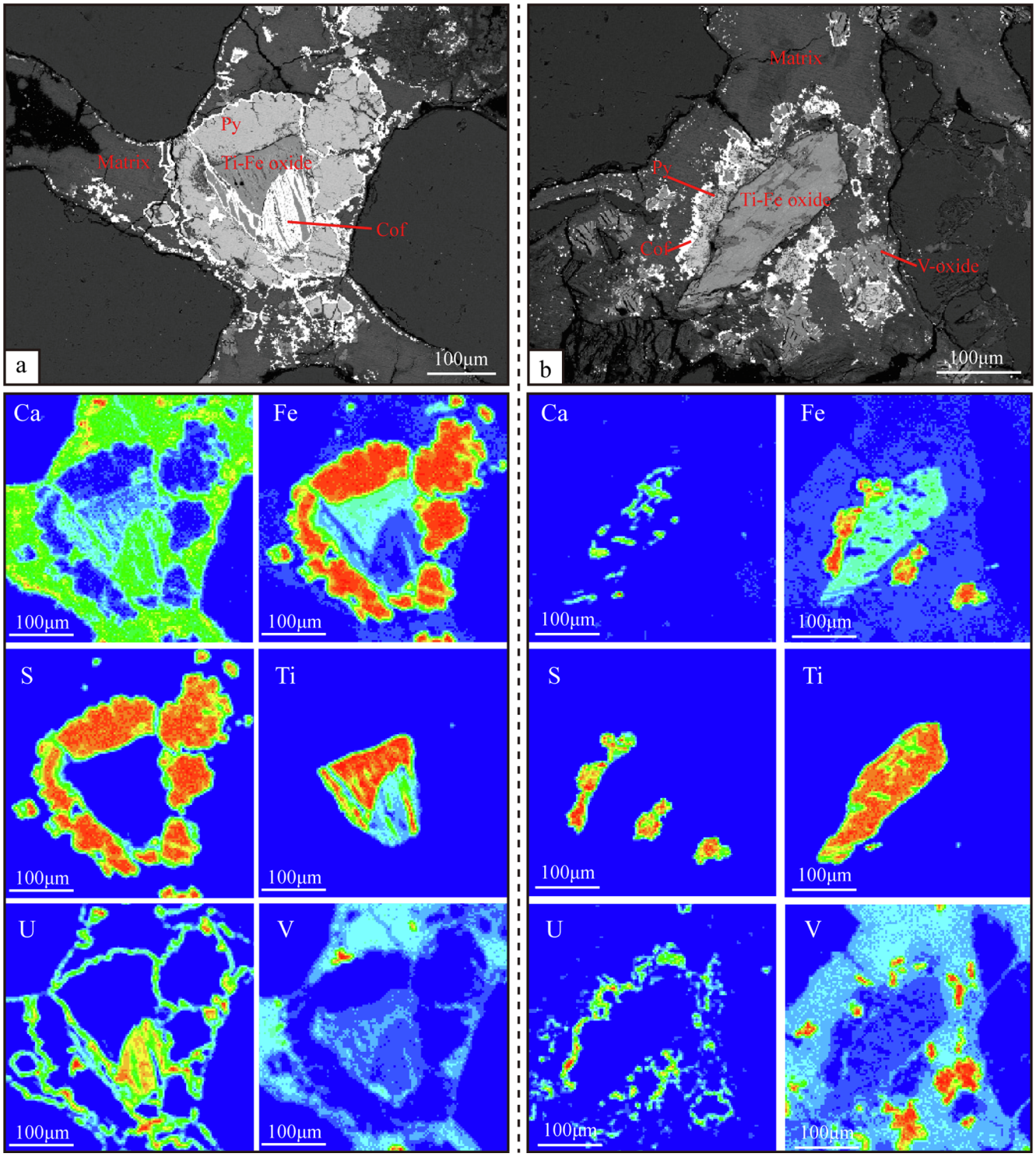

Fig. 10. Spatial relationships and mineral chemical information of the pyrites, Ti-Fe oxides, with the EDS area scans of relevant elements (Ca, Fe, S, Ti, U, and V).

minerals on the periphery of clay minerals suggests the adsorption of U on clay minerals and their role as catalysts for the reaction between oxidized uranium fluids and reducing fluids. Presence of uranium minerals on the periphery of the pyrites, carbon debris, and fossils indicates the contribution of reducing media to the reduction–precipitation–enrichment of U in oxidized fluids.

7. Discussion

7.1. Genetic order of the main altered minerals

In the study, morphological characterization has helped to determine the genetic order of the achavalites, pyrites, carbonates, and uranium minerals in the sandstone-type uranium deposits in the North Ordos Basin.

In the diagrams of Fig. 15, which show the precipitation of Se, U, V, and pyrites at different Eh and pH intervals, as reported in Максимова

Table 2
Geochemical data obtained by EMPA for pyrites and achavalite in the uranium deposits of North Ordos Basin

Sample No.	Sample Description	Data No.	Component (WT(%))									
			As	Se	S	Fe	Pb	Cu	Zn	U	Ti	Total
WN5-17	Gray-green sandstone	1	0.383	13.138	42.161	43.964	0	0.06	NULL	0.014	0.063	99.78
		2	0.06	68.963	2.058	27.82	0	0	NULL	0.007	0	98.91
		3	0.217	23.625	33.776	41.376	0	0	NULL	0.024	0.022	99.04
		4	0.081	66.923	4.629	28.646	0.014	0	NULL	0.023	0.018	100.33
		5	0.276	1.911	47.223	47.009	0	0.033	NULL	0.095	0.017	96.56
		6	0.063	65.286	6.499	29.107	0	0.044	NULL	0.04	0	101.04
		7	0.256	2.174	49.495	46.528	0	0	0.053	0	0.007	98.51
		8	0.016	68.451	3.252	28.546	0	0.048	0.065	0.003	0.019	100.40
		9	0.044	68.089	4.402	28.371	0	0	NULL	0	0	100.91
		10	0.302	1.11	50.684	47.752	0	0.044	0	0.003	0	99.90
		11	0.253	0.802	50.002	47.305	0	0.056	0	0.048	0.003	98.47
		12	0.056	67.899	4.249	28.405	0	0.024	0	0	0.001	100.64
		13	0.032	60.563	4.892	28.693	0	0.042	0.096	0.03	0.017	94.36
		14	0.085	71.415	3.29	27.783	0	0	NULL	0.013	0.012	102.60
		15	0.06	67.658	4.082	28.609	0	0	0.036	0.042	0	100.49
		16	0.291	0.021	51.574	47.625	0	0.051	0	0.033	0.004	99.60
		17	0.004	66.002	4.849	29.038	0	0.024	NULL	0.026	0.002	99.94
WTN7-52	Gray-white sandstone	1	0.305	0	47.739	46.846	0	0.027	NULL	0.052	0.011	94.98
		2	0.188	0	48.529	47.301	0	0	NULL	0.012	0	96.03
		3	0.301	0	47.705	47.248	0	0.281	NULL	0.194	0.006	95.74
		4	0.461	0.016	46.724	46.28	0	0.047	NULL	0.037	0.001	93.57
		5	0.433	0.038	44.611	45.646	0	0.035	NULL	0.016	0.005	90.78
		6	0.41	0	45.381	44.862	0	0.068	NULL	0.012	0	90.73
		7	0.289	0	49.112	47.558	0	0.047	NULL	0	0.025	97.03
		8	0.311	0	46.323	46.645	0	0.006	NULL	0.038	0.013	93.34
		9	0.333	0	48.008	47.54	0	0	NULL	0.007	0.016	95.90
		10	0.276	0	47.079	47.371	0	0.07	NULL	0.03	0	94.83
ZK12-62	Gray sandstone	1	0.313	0.101	48.613	45.737	0	0.031	NULL	0.005	0.004	94.80
		2	0.461	3.135	47.731	43.362	0	0.017	0.015	0.008	NULL	94.73
ZK25-2	Gray-white sandstone	1	0.3	0	50.318	45.525	0	0	0.039	0	NULL	96.18
ZK17-5	Gray-white sandstone	1	0.264	0.003	50.88	46.986	0	0	0.074	0.008	0.012	98.23
		2	0.266	0.115	50.62	46.891	0.008	0	0	0.043	0	97.94
		3	0.249	0.353	48.738	46.747	0	0	0.044	0.017	0	96.15
		4	0.248	0.74	50.876	46.88	0	0.009	0.064	0.072	0	98.89
ZK17-6	Gray-white sandstone	1	0.324	0	51.556	46.444	0	0.036	0	0.017	0	98.38
ZK17-7	Gray-white sandstone	1	0.244	0.412	52.468	47.248	0	0.012	0.064	0	0	100.45
		2	0.25	9.052	45.029	43.134	0.003	0.018	0.064	0.025	0.013	97.59
ZK17-8	Gray-white sandstone	1	0.218	1.549	51.178	47.246	0	0.008	0.079	0.019	0.019	100.32
44-131-t1	Gray-white sandstone	1	0.188	0.133	52.687	49.394	0	0	0.034	0.023	0	102.46
		2	0.134	6.867	47.638	47.611	0	0	0.029	0.008	0	102.29
		3	0.236	0.543	52.685	48.763	0	0	0	0	0	102.23
		4	0.152	3.446	50.389	47.843	0	0	0.011	0	0	101.84
44-131-t2	Gray-white sandstone	1	0.17	0.038	51.745	49.344	0	0.06	0.023	0.001	0	101.38
		2	0.196	0	52.433	49.692	0	0	0	0.016	0	102.34
		3	0.145	0	52.361	49.806	0	0.059	0.028	0	0	102.40
		4	0.155	0	51.926	48.876	0	0.085	0	0.081	0	101.12
		5	0.171	0.001	51.955	49.624	0	0	0	0	0	101.75
		6	0.193	0	50.873	48.129	0	0.006	0.007	0.016	0	99.22
44-131-t3	Gray-white sandstone	1	0.192	0	52.878	49.021	0	0	0.012	0.004	0	102.11
		2	0.169	0	52.089	49.663	0	0.017	0	0	0	101.94
		3	0.151	0	52.821	48.708	0	0.065	0.052	0.045	0	101.84
44-131-t4	Gray-white sandstone	1	0.13	7.301	42.135	43.986	0	0.016	0	0	0	93.57
		2	0.186	0.02	50.712	46.206	0	0.014	0	0.021	0	97.16
		3	0.178	0	52.271	49.017	0	0	0.022	0	0	101.49

and Шмариович (1993), as Eh reduces, achavalites and pyrites precipitate earlier than the uranium minerals. Although in water solutions, Fe-Se compounds precipitate in similar conditions to those of Fe-S compounds, Se precipitates earlier than S in a weakly acidic environment, as evidenced by the development of pyrites that envelop the achavalites. When the solution becomes weakly alkaline, the precipitation field of Se overlaps with that of S, resulting in pyrites enveloping and being enveloped by achavalites or occurring in zonal form. In Nalinggou deposit, the achavalites are mostly enveloped by pyrites (Fig. 9-a), except in a couple of the samples, in which achavalites are hosted in pyrites in zonal form. This suggests that the achavalites formed earlier than the pyrites; the solution pH was weakly acidic at the time of their formation, although they became weakly alkaline later on with the development of carbonates. Since the achavalites and pyrites precipitated earlier than the uranium minerals, their U contents are very low. The uranium minerals mostly occur around the achavalites and pyrites, and are rarely observed to interweave with each other. In a couple of the samples, V is hosted in a matrix around the pyrites and enveloped by uranium minerals. The Ti-Fe oxides, which had initially existed as detrital minerals, were subsequently altered. Without changing the original crystal morphology, Fe gradually removed or was replaced by Ca or U, giving rise to halo textures. The precipitated Fe reacted with H_2S on the periphery of the Ti-Fe oxides to generate pyrite. The uranium migrated in oxygenated fluids mostly as carbonate complexes (Christina and Cochran, 1993; Di, 2002; Liu et al., 2006c; Feng et al., 2016; Wu et al., 2016). As a chemical reaction took place on the redox interface, uranium precipitation was accompanied by the development of HCO_3^- and CO_2, which,

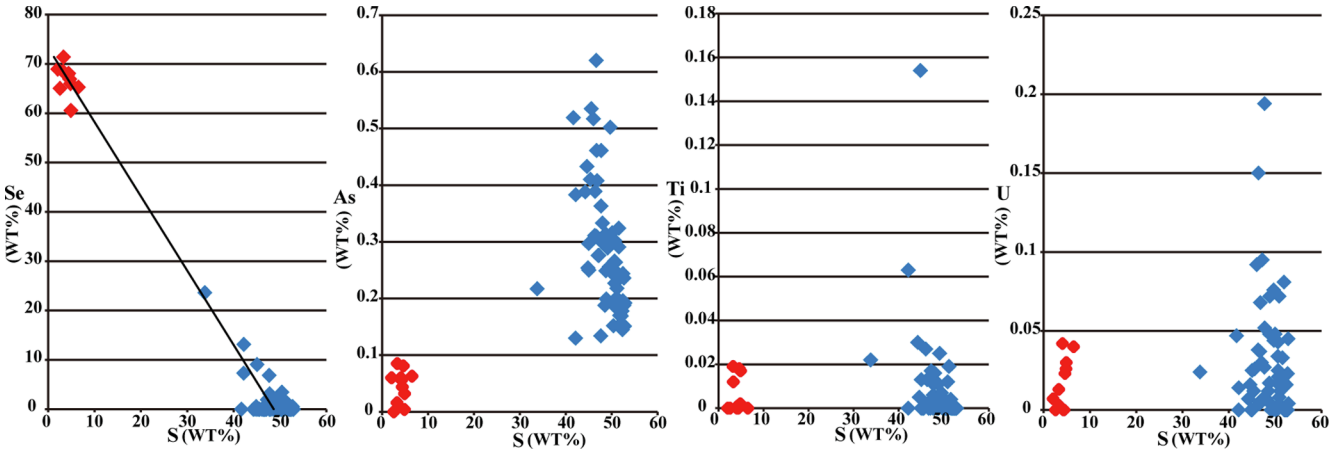

Fig. 11. Mineral chemical plots of Se, As, Ti, U versus S for pyrites and achavalites (Red plot-Achavalite; Blue plot-Pyrite). (For interpretation of the references to color in this figure legend, the reader is referred to the web version of this article.)

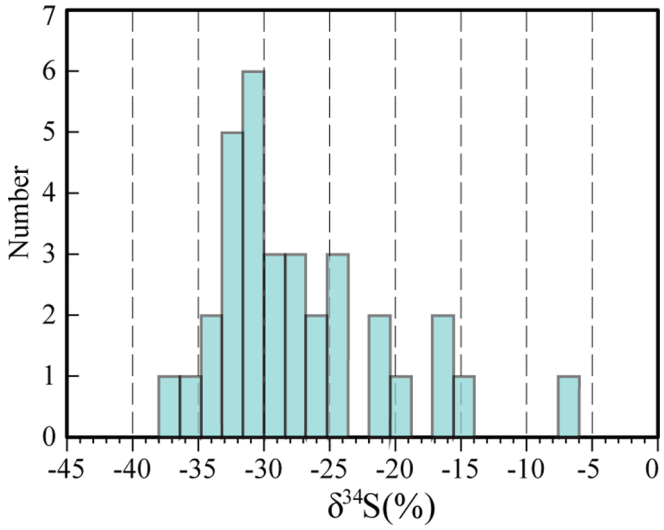

Fig. 12. Pyrite S isotope data form of the deposits in the Northe Ordos Basin.

together with the Ca^{2+} in the oxygenated uranium fluids and the surrounding matrixes, generated $CaCO_3$. This explains why carbonate cements are frequently found in the uranium mineral-enriched areas.

Furthermore, the morphological characteristics of the altered minerals, and the low U content of the achavalites and pyrites, as discussed above, also confirm the genetic order of the main altered minerals during the metallogenic stage to be achavalite > pyrite > vanadium compounds > uranium minerals > carbonates.

7.2. Uranium mineralization during basin evolution

Since the Mesozoic, the study area has undergone basin sedimentation and subsidence, Cretaceous tectonic inversion, and Paleogene Hetao rifting (Liu, 2005; Yang et al., 2015; Zhao et al., 2016). These events are respectively responsible for the original pre-enrichment of uranium minerals, the coupling of oxygenated uranium fluids and reducing fluids, and the disconnection of the metallogenic areas from the uranium sources. They also account for the development of ore-bearing altered minerals in different time periods.

The Middle Jurassic Yan'an Formation, which comprises swamp or fluvial deposits, is a formation of gray sandstone and numerous black coalbeds developed in a strongly reducing environment. The widespread colloidal spherical pyrites and vein-like pyrites there provided ample detrital pyrites and carbon debris for the overlying Lower Zhiluo Formation.

The Middle Jurassic Zhiluo Formation formed in a giant braided river depositional system, that overlies the Yan'an Formation in angular unconformity, due to compression during the early Yanshanian Movement. In the North Ordos Basin, the Zhiluo Formation provides a high-quality ore-hosting bed for sandstone-type uranium ores (Jiao et al., 2005). There are large inter-layers of mudstone-sandstone-mudstone, meanwhile sandstones have the high permeability which would act as the flow pathway, and organic matters which would be the reduce materials. In the Daqingshan orogen in the north, there are numerous uranium-rich lithologies (e.g., the Dahuabei) and extensive gold and pyrite-hosting quartz veins (e.g., the Hadamengou gold deposit) (Zhang et al., 2006; Chen et al., 2017b). In the early diagenetic stage, the formation was originally pre-enriched as aggregates of detrital grains containing some uranium minerals. Pyrites from the underlying formation, which had formerly existed as irregular detrital grains, were subsequently preserved in the original reducing environment of the Zhiluo Formation (Zhang et al., 2016b; Sun et al., 2017). The extensive Ti-Fe oxides contained in these detrital grains provided material sources for the subsequent enrichment of uranium minerals and pyrites (Chen et al., 2017a; Fang and Li, 2017). The development of mica minerals, on the other hand, provided space and absorption locations for the precipitation of pyrites and uranium minerals (Miao et al., 2009; Chen et al., 2017b). In the diagenetic stage, micritic calcites cemented the detrital grains to form the earliest carbonates of the Zhiluo Formation. These carbonates, however, are not directly responsible for the formation of the sandstone-type uranium deposits as they reduced the porosity and permeability of the sandstones and therefore impeded the subsequent infiltration of oxidized uranium fluids. Nevertheless, development of some colloidal and framboidal pyrites during the same period (Figs. 5 and 16) provided important reducing for the subsequent enrichment of uranium minerals (Ingham et al., 2014; Chen et al., 2016; Zhang et al., 2017a). In addition, the clay mineral overgrowth membranes on the surfaces of the detrital grains also provided important locations for subsequent uranium mineralization (Song et al., 2016; Chen et al., 2017b).

At the end of the Jurassic, the Bo'erjianghaizi fault zone cut the Zhiluo Formation, thus providing important structural fracture pathways for the subsequent upward migration of deep oil and gas (Yang et al., 2013, 2015).

Due to regional compression during the Cretaceous, the depocenter of the basin underwent an inversion, accompanied by the development of fault structures. The northeast area of the basin was elevated, causing the depocenter to shift to the west (Liu et al., 2006; Li et al., 2012; Zhao et al., 2012). This Yanshanian Movement caused the Jurassic and

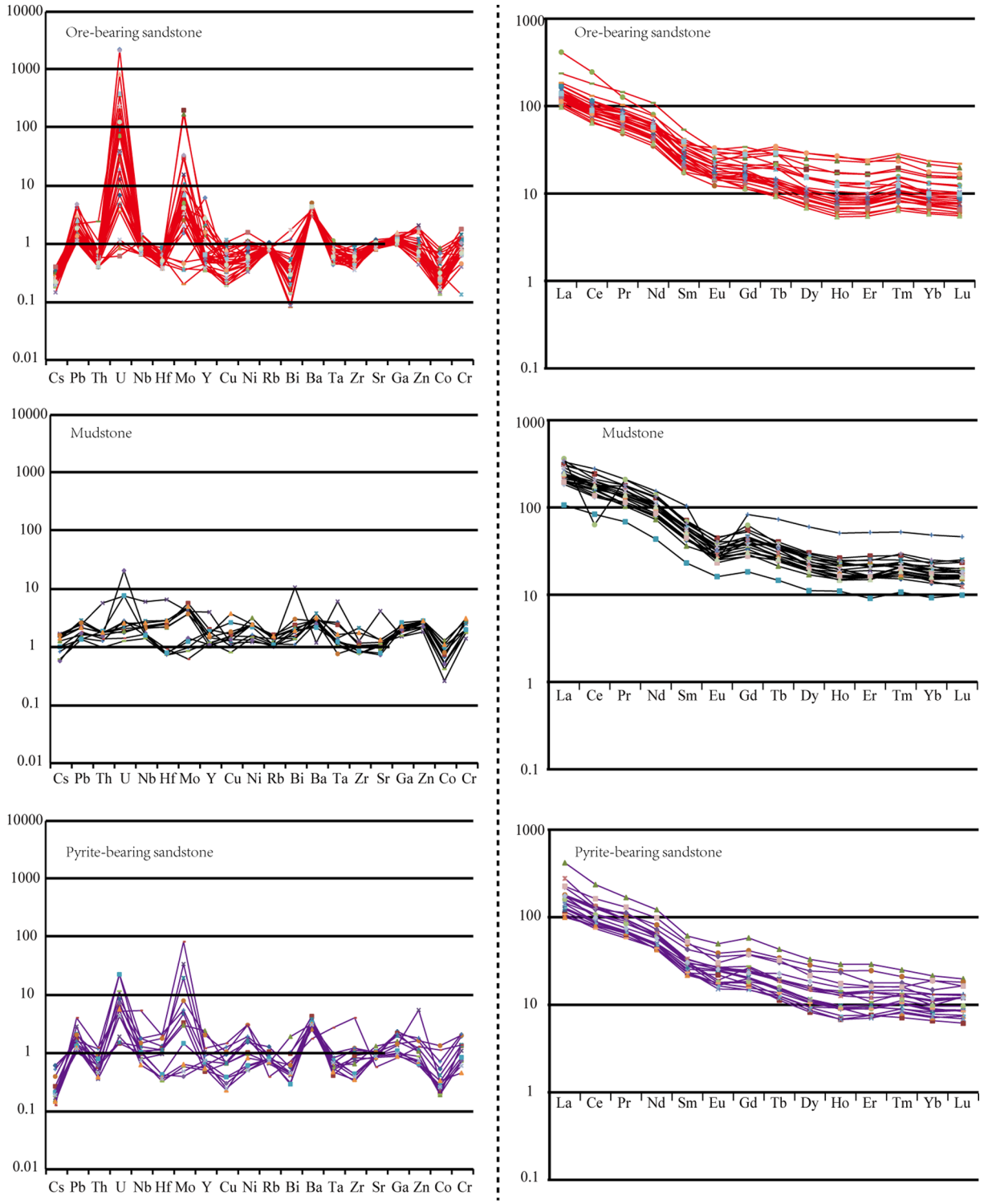

Fig. 13. Mineral chemical spider diagrams, including the Trace elements, and REEs of the deposits in the Northe Ordos Basin.

earlier formations in the northeast area of the basin to rise toward the earth's surface, thereby providing material sources for the Cretaceous and more recent overlying stratum. Subsequently, oxidized uranium-bearing fluids migrated downward along the elevated formations in the northeast. Given that uranium in these formations had been pre-enriched (Xia and Liu, 2005; Chen et al., 2017b), in addition to the uranium elements from the provenance, the oxidized uranium-bearing fluids facilitated the further migration of uranium in the formations, subsequently resulting in enrichment–mineralization where the redox interfaces were encountered. In the meantime, the earlier pyrites in the formations, affected by the oxygenated fluids, were oxidized to goethite or hematitite in the oxidation zones.

The late Early Cretaceous to the Late Cretaceous was the main metallogenic period for epigenetic sandstone-type uranium deposition in the North Ordos Basin, which typically occurred between 125 Ma and 84 Ma (Xia et al., 2003a,b; Liu et al., 2012). This is also the main development period for the colloidal pyrites, colloidal calcites, and intergranular chlorites. Also, due to the regional extension, deep

Table 3
Geochemical data obtained by EMPA for uranium minerals in the Nalinggou uranium deposit, Ordos Basin, China.

Sample and Test Point No.		Test Result in wt%														
		Na_2O	SiO_2	UO_2	FeO	Al_2O_3	MgO	CaO	TiO_2	Y_2O_3	SO_3	K_2O	PbO	ZrO_2	P_2O_5	Total
zk4	1	0.56	19.81	58.46	0.65	1.47	0.93	2.19	0.16	6.36	0.11	0.24	/	/	1.23	92.17
	2	0.36	19.33	62.54	0.43	1.04	0.21	1.93	1.74	5.60	0.31	0.17	/	/	1.23	94.89
	3	0.18	19.83	59.76	2.46	1.20	0.11	0.50	0.30	3.87	2.29	0.28	/	/	0.71	91.49
zk7	1	0.43	19.25	64.83	0.23	1.56	0.21	2.62	1.56	1.28	0.04	0.24	/	0.37	0.43	93.31
	2	0.39	19.57	70.58	0.23	1.37	/	2.09	/	0.62	/	0.20	0.10	/	0.31	95.46
	3	0.21	20.45	63.55	0.24	1.70	0.05	2.03	2.39	1.37	/	0.17	/	0.23	0.56	92.95
	4	0.67	20.44	62.50	0.27	1.79	0.16	2.50	1.00	1.00	0.02	0.19	/	0.23	0.45	91.22
	5	0.93	20.35	66.92	0.49	1.51	0.11	1.92	0.32	1.05	0.10	0.21	/	/	0.44	94.35
zk19	1	*0.50*	*4.74*	*85.04*	*0.93*	*0.38*	/	*4.14*	*0.80*	/	/	*0.25*	*0.20*	*0.09*	*0.08*	*97.15*
	2	*0.56*	*3.91*	*87.47*	*0.87*	*0.38*	*0.03*	*4.00*	/	/	/	*0.23*	*0.09*	/	*0.22*	*97.76*
	3	*0.98*	*4.09*	*85.35*	*1.09*	*0.28*	*0.02*	*4.77*	*0.46*	/	/	*0.29*	/	/	*0.13*	*97.46*
	4	0.34	20.02	70.48	0.44	1.39	0.04	2.41	0.13	0.32	0.04	0.20	/	0.07	0.78	96.66
zk42	1	0.54	20.33	56.80	0.54	1.11	0.04	1.49	0.22	7.30	0.51	0.21	0.14	/	0.90	90.13
zk48	1	0.62	20.95	64.65	0.16	1.41	0.05	2.21	0.21	2.22	/	0.20	0.20	/	0.49	93.47
	2	0.22	19.06	64.73	0.98	1.01	0.03	1.95	3.41	2.02	0.02	0.17	0.11	/	0.41	94.12

hydrocarbon-bearing fluids continued to migrate upward along fault structures, thus providing reducing media and subsequent preservation of uranium mineralization. The discovery of the numerous oil sand resources in the Cretaceous Dongsheng Formation in northern Dongsheng (Xue et al., 2011) is evidence of the extensive oil–gas processes that operated in the North Ordos Basin after the early Late Cretaceous. Extensive upward oil–gas migration altered the Eh and pH conditions at the redox interfaces, and resulted in the mineral paragenesis of achavalite > pyrite > uranium minerals > carbonates.

These deep-source hydrocarbon-bearing fluids (including oil gases and coalbed methanes) provided abundant reducing agents and S for the formation of pyrites in this area. They were also important reducing agents for the precipitation of U (Wang and Du, 1995; Yang et al., 2006; Chen and Guo, 2007; Cai et al., 2008; Wu et al., 2016; Hall et al., 2017; Jiao et al., 2018).

Typically, the restrictions of the hydrocarbon fluids to the areas of uranium mineralization are reflected by the contributions of H_2, CH_4, CO, and H_2S to the reduction of uranium:

$$UO_2^{2+} + H_2 \rightarrow UO_2 + 2H^+$$

$$4UO_2^{2+} + CH_4 + 3H_2O \rightarrow 4UO_2 + HCO_3^- + 9H^+$$

$$UO_2^{2+} + 2CO + H_2 + H_2O \rightarrow UO_2 + C + HCO_3^- + 3H^+$$

$$4UO_2^{2+} + H_2S + 10OH^- \rightarrow 4UO_2 + SO_4^{2-} + 6H_2O$$

$$UO_2 + H^+ + SiO_2 \rightarrow USiO_4 + UO_2^{2+} + H_2O$$

In addition, in drill core through the Zhiluo Formation, numerous faults in the yellow oxidized sandstone provided pathways for the upward migration of these hydrocarbon-bearing fluids. The combination of hydrocarbon-bearing fluids with the oxidized fluids on the surface of the faults produced sheet-like pyrites, resulting in chloritization on the upside, although the original yellow coloration was retained on the downside (Fig. 3-K&I). This further confirms the significant role played

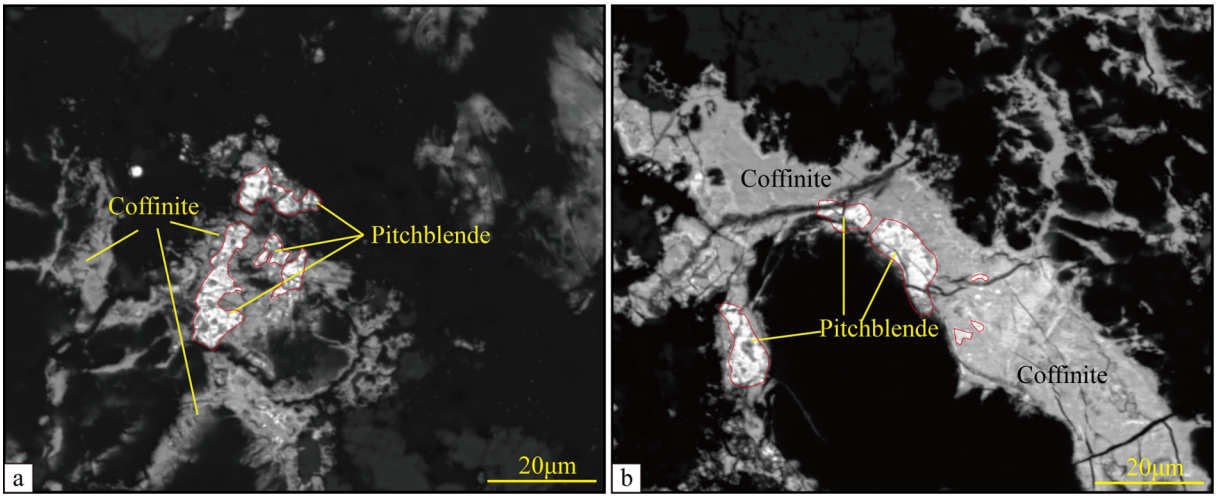

Fig. 14. Spatial relationship between coffinite and pitchblende.

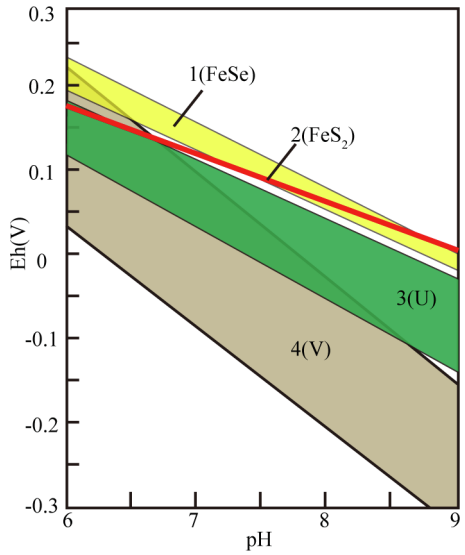

Fig. 15. Eh-Ph diagrams showing theoretically-calculated reductive precipitation fields for some of the uranium-related elements in natural water (T = 25 °C, P = 0.1 MPa) (modified after Максимова М.Ф., ШмариовичЕ. М., 1993; Chen and Guo, 2007) 1- Se precipitated as Se solid with activity drop ranging 10^{-6}–10^{-9}; 2- balance line of geothites + esmeraldaites - pyrites (area below the line) 3- U precipitated as UO_2 (10^{-6}–10^{-9}); 4-V precipitated as parafrovanite (10^{-5}–10^{-8}).

by oil and gas in the North Ordos Basin in the later stage of uranium mineralization.

In the Paleogene, the development of the Hetao rift in the North Ordos Basin disconnected the Daqingshan uranium sources and the provenance from the deposits. The subsequent metallogenesis primarily occurred by the migration of early uranium mineralization as roll fronts (Hou et al., 2017), which existed mainly as coffinite. With the continued uplift of the northern margin of the Ordos basin, the Cretaceous, Jurassic, and other formations were exposed to the surface and suffered the denudation. The oxide water flowed down and met with the pre-existing uranium ore body. The U^{4+} will be oxidized into U^{6+}, and migrated with the flow until met with the reduced material to be reduced and concentrated to be the new uranium ore body. Most of these ore bodies are located in the front of the earlier bodies. While the mineralization was migrating forward, the pyrites were also being hematized or cemented by calcites. The REE distribution in the uranium orebodies and the vertically adjacent country rocks also indicates that U is more enriched in the ore-bearing sandstones and pyrite-bearing sandstones than in the mudstones, and verifies that ore-bearing fluids were further enriched in sandstone.

In the sandstone-type uranium deposits of the North Ordos Basin, two kinds of uranium minerals are found, pitchblende and coffinite (Fig. 14). The crystallization of pitchblende and coffinite are influenced by pH, Eh, and activity coefficient of SiO_2 (ДамковЮ, 1973; КомовИЛ, 1982; Cuney et al., 1991; Min et al., 1999; Wang et al., 2017). Pitchblende prefers to crystalize under conditions of neutral-weak acidity and weak oxidation/weak reduction potential, with the activity coefficient of $SiO_2 < 10^{-3.5}$ mol/L H_2O (Wang et al., 2017 and references therein). Coffinite mainly concentrates in neutral-weak alkaline conditions with stronger reduction potential, and the activity coefficient of $SiO_2 \geq 10^{-3.5}$–$10^{-2.7}$ mol/L H_2O (Wang et al., 2017 and references therein). With the increase of the activity coefficient of SiO_2 in the fluid, pitchblende (UO_2) incorporates Si to form coffinite (nominally U $(SiO_4)\cdot nH_2O$) (РафальскийРП, 1963; Wang et al., 2017). At the end of Cretaceous, the North Ordos basin was uplifted and experienced denudation. With the Zhiluo Formation exposed at the surface, a complete hydrodynamic system was formed. The fluid from the orogenic belt is rich in oxygen and uranium contents, and reacted with Fe-sulphides (pyrites) and organic materials in the Zhiluo Formation. A large amount of CO_3^{2-} and SO_4^{2-} ions are formed and cause the fluid to become weakly acidic. Under the acid conditions, the activity coefficient of SiO_2 is lower, which is favorable for the formation of pitchblende. However, in the Late Cretaceous, activities of various hydrocarbon-bearing fluids increased and, following the intrusion of these hydrocarbon-bearing fluids into the host rock, a variety of alteration features formed in the ore-bearing layer, for example chlorite (Wu et al., 2006). During the alteration process, a large amount of K^+ and $Fe^{2+/3+}$ ions were released and reacted with CO_3^{2-} in the fluid to form K_2CO_3 which forced the geochemical environment to change from acid to alkaline, with the pH values between 6.7–10 (Chen et al., 2006; Wu et al., 2007). Under these alkaline conditions, the original pitchblende transformed into coffinite. In the Late Paleogene, the Hetao rift developed at the northern margin of the Ordos basin, the original hydrodynamic system was broken, and the surface runoff changed from the basin to the Hetao rift (Chen et al. 2006). The Zhiluo Formation then only had little groundwater recharge from the rainfall. As a result, the alkaline situation persisted for a long period, which benefited coffinite formation. As presented in the Fig. 14, pitchblendes are surrounded by coffinites. In addition, the isotopic chronology of uranium minerals indicates that the metallogenesis of uranium deposits in the North Ordos basin are multi-stage, over a large time span (177–9.8 Ma) (Liu et al., 2012; Zhang et al., 2018). Within that time span, two peak metallogenic epochs can be recognized, 124–65 Ma and 22–8 Ma when the coffinite mainly formed (Liu et al., 2012).

7.3. Constrains of pyrite to uranium mineralization

The results of S isotope analysis of the pyrites reveal that, in the redox transition zones of the North Ordos Basin, the widespread sulfate-reducing bacteria consumed hydrocarbon fluids inside the formations or from the deep levels. The consequent enrichment of H_2S in the formations gave rise to pyrites and other metal sulfides, accompanied by the precipitation–enrichment of uranium minerals. In addition, the earlier pyrites in the formations could also have generated H_2S after reacting with water in the oxygen-free media (Chen and Guo, 2007). With the formation of H_2S, the redox potential has a steep reduction, which enhanced the precipitation–enrichment of pyrites and uranium minerals. Fig. 15 shows that pyrite requires a higher redox potential than uranium minerals. While Eh was reduced, Fe^{3+} precipitated earlier than U^{6+}, which explains why the uranium minerals that are observed around fresh pyrites. Further work, however, is needed to determine whether H_2S or FeS_2 acted as the reducing agent in the redox precipitation of uranium. Overall, their contributions to uranium reduction can be expressed as follows:

H_2S to Fe^{3+} and U^{6+}:

$$2Fe_2O_3\cdot H_2O + 6H_2S \rightarrow FeS + Fe_3O_4 + S + 8H_2O$$

$$FeS + H_2S \rightarrow FeS_2 + 2H^+$$

$$4UO_2^{2+} + H_2S + 10OH^- \rightarrow 4UO_2 + SO_4^{2-} + 6H_2O$$

FeS_2 to U^{6+}:

$$7UO_2^{2+} + FeS_2 + 8H_2O \rightarrow 7UO_2 + Fe^{2+} + 2SO_4^{2-} + 16H^+$$

$$UO_2^{2+} + Fe^{2+} + 3H_2O \rightarrow UO_2 + Fe(OH)_3 + 3H^+$$

$$[UO_2(CO_3)_3]^{4-} + 2Fe^{2+} + 3H_2O \rightarrow UO_2 + 2Fe(OH)_3 + 3CO_2$$

Coffinite represents the main uranium mineral in these sandstone-type uranium deposits, which differs from the pitchblende in the deposits of the Yili, Erlian, and Songliao Basins (Yang et al., 2009b; Liu et al., 2013; Bonnetti et al., 2015; Chen et al., 2017a,b), although a small amount of star-like pitchblende in some samples are observed. Compared with other basins in North China, the uranium provenance is disconnected from the deposits because of Hetao rifting in the North

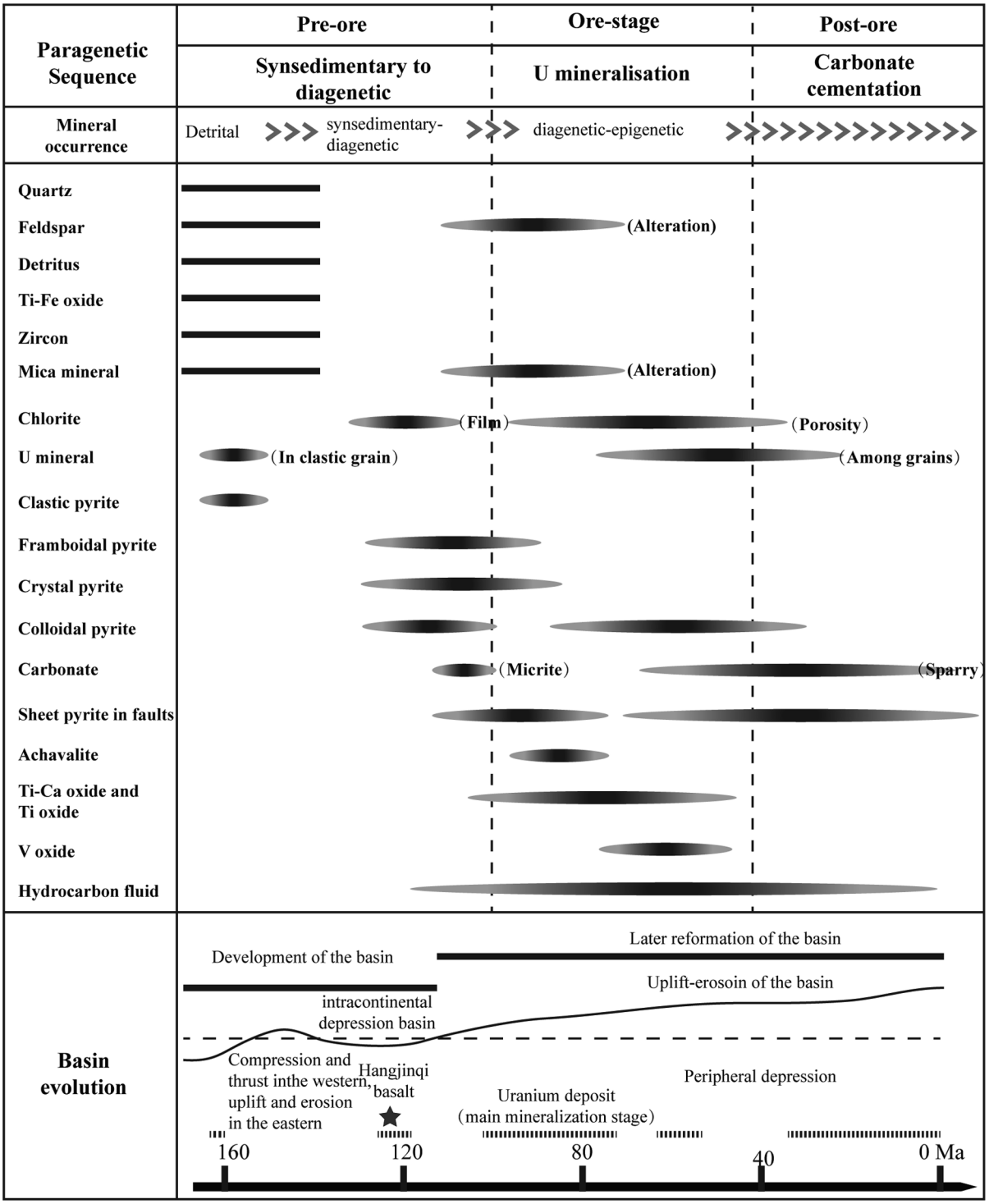

Fig. 16. Paragenetic sequence for the main detrital, alteration, and ore minerals in the sandstone-type uranium deposits in the North Ordos Basin (modified after Xia et al., 2003a,b; Liu et al., 2006b; Xiang et al., 2006b; Xing et al., 2006; Zhang et al., 2015; Bonnetti et al., 2017).

Ordos Basin during the Paleogene (Gao and Yu, 1990; Wang, 2017). Then, with the movement of the oxygenated water, the early mineralizations migrated forward to deeper levels (Spirakis, 1996). However, more study is needed to determine why the uranium mineralizations in this area exist as coffinite, rather than pitchblende.

8. Conclusions

By using EPMA, SEM, and isotopic geochemical analysis, the morphology, composition, and S isotopes of the pyrites in the uranium deposits of North Ordos Basin, China, were systematically investigated. By discussing the regional tectonic evolutionary sequence of the basin, the relationships between the pyrites and uranium mineralization were further determined.

1. The morphologies of the pyrites in the uranium deposits are characterized macroscopically and microscopically. Macroscopically, the pyrites occur in lumpy, banded, disseminated, star-like or sheet-like form. Microscopically, they exist either as detrital grains or inside detrital grains, as idiomorphic grains, in colloidal or framboidal

form, inside mica minerals, in banded or petaloid form, or in other forms related to biological cells or microorganisms.

2. The genetic order of the main altered minerals in the uranium deposits is: (a) during the diagenetic stage - detrital pyrites > clay mineral overgrowths/membranes > micritic calcites; (b) during the metallogenic stage - achavalites > pyrites > uranium minerals > vanadium oxides > sparry calcites.
3. It is found that the pyrites and achavalites have very low U contents, with the pyrites containing more U than the achavalites. The $\delta^{34}S$‰ values, even in the pyrites, is highly variable (−7.3‰ to −37.2‰), but principally in the proximity of −30‰, and display obvious biogenic characteristics. If sulfate-reducing bacteria consumed hydrocarbon fluids, the formations would have become rich in H_2S, which could have changed the Eh level of the formations and encourage the precipitation of pyrites and uranium minerals.
4. During basin evolution, the Yan'an Formation served as an important pyrite and organic provenance for the overlying formations. During the deposition of the Zhiluo Formation, pyrites typically existed as detrital grains, spherical colloidal pyrites, and framboidal pyrites. The Cretaceous was the main metallogenic period for epigenetic uranium deposition in the study area. It was also the main development period of the pyrites accompanying the upward oil–gas migration, which mainly occurred as colloidal pyrites closely associated with the redox reaction of uranium mineralization.
5. Remobilization of uranium occurred in the Paleogene, when the development of the Hetao rift in the north disconnected the sedimentary material and the uranium sources from the deposit areas. At this time, uranium mineralization mainly occurred by roll front migration of early uranium mineralization.

Acknowledgments

This study was jointly supported by National Key Basic Research Program (grant No. 2015CB45300), National Science Foundation for Young Scientists (grant No. 41502195), and National Key R&D Program of China (grant No. 2018YFC0604200) from the Ministry of Science and Technology of China, and Geological Suevey Project (grant No. DD20160127) from China Geological Survey. We appreciate the CNNC Beijing Research Institute of Uranium Geology for their assistance in Trace elements, REE and S isotopic analyses. We thank Dr. Franco Pirajno, Dr. Zenghua Li and two anonymous reviewers for their constructive comments and suggestions on the manuscript. We also thank editorial employees to edit the paper.

References

Akhtara, S., Yang, X.Y., Pirajno, F., 2017. Sandstone type uranium deposits in the Ordos Basin, Northwest China: A case study and an overview. J. Asian Earth Sci. 146, 367–382.

Bonnetti, C., Cuney, M., Malartre, F., Michels, R., Liu, X.D., Peng, Y.B., 2015. The Nuheting deposit, Erlian Basin, NE China: Synsedimentary to diagenetic uranium mineralization. Ore Geol. Rev. 69, 118–139.

Bonnetti, C., Liu, X.D., Yan, Z.B., Cuney, M., Michels, R., Malartre, F., Mercadier, J., Cai, J.F., 2017. Coupled uranium mineralisation and bacterial sulphate reduction for the genesis of the Baxingtu sandstone-hosted U deposit, SW Songliao Basin, NE China. Ore Geol. Rev. 82, 108–129.

Cai, C.F., Li, H.T., Luo, X.R., 2005. Petroleum related origin for sandstone-hosted uranium deposits in the Dongsheng area, Ordos Basin (China). In: Mao, J.W., Bjerlein, F.P. (Eds.), Mineral Deposit Meeting the Global Challenge-Proceedings of the 8th Biennial Society for Geology Applied to Mineral Deposits Meeting. Springer Verlag, Berlin, pp. 229–302.

Cai, C.F., Li, R.X., Qin, M.K., Luo, X.R., Wang, F.Y., Ou, G.X., 2007. Biogenic and petroleum-related ore-forming processes in Dongsheng uranium deposit, NW China. Ore Geol. Rev. 32, 262–274.

Cai, C.F., Li, H.T., Li, K.K., Jiang, L., 2008. Anaerobic oxidation of petroleum coupled with reduction of uranium mineralization-cases from Dongsheng and Qianjiadian Uranium Deposits. Petrol. Geol. Exp. 30 (5), 518–521 (in Chinese with English abstract).

Chen, L.L., Feng, X.X., Sima, X.Z., Li, J.G., Guo, H., Chen, Y., Zhao, H.L., Tang, C., Wang, G., Liu, Z.R., Li, S.G., 2017a. Occurrence forms of the uranium minerals in the Nalinggou area of the ordos basin and geological implications. Geol. Explor. 56 (4), 632–642 (in Chinese with English abstract).

Chen, Y., Feng, X.X., Chen, L.L., Jin, R.S., Miao, P.S., Sima, X.Z., Miao, A.S., Tang, C., Wang, G., Liu, Z.R., 2017b. An analysis of U-Pb dating of detrital zircons and modes of occurrence of uranium minerals in the Zhiluo Formation of northeastern Ordos Basin and their indication to uranium sources. Geol. China 44 (6), 1190–1206 (in Chinese with English abstract).

Chen, Z.Y., Guo, Q.Y., 2007. Mechanism of U-reduction and Concentration by Sulphides at Sandstone type Uranium Deposits. Uran. Geol. 23 (6), 321–327 (in Chinese with English abstract).

Chen, C., Liu, H.J., Hou, H.Q., Han, S.Y., Ke, D., Bai, Y.S., Ou, G.X., Li, Y.R., 2016. The Relationship between Pyrite and Sandstone-hosted Uranium Mineralization of the Zhiluo Formation in the Northern Ordos Basin. ACTA Geol. Sin. 90 (12), 3375–3380 (in Chinese with English abstract).

Chen, F.Z., Zhao, J.F., Chang, B.C., Gao, J.Y., 2006. A prel iminary analysis and assessment of hydrogeological conditions for in-situ leach mining of sandstone-type uranium deposit in northern Ordos basin. Uran. Geol. 22 (3), 163–167 (in Chinese with English abstract).

Christina, E.B., Cochran, J.K., 1993. Uraniumgeochemistry in estuarine sediments: Controls on removal and release processes. Geochim. Cosmochim. Acta 57 (3), 555–569.

Cuney, M., Pechmann, V.E., Rimsaite, J., Simova, F., Sorensen, H., Augutithis, S.S., 1991. Primary Radioactive Minerals. Theophrastus Publications. S. A, Greece, pp. 235–254.

Dai, S.F., Yang, J.Y., Ward, C.R., Hower, J.C., Liu, H.D., Garrison, T.M., French, D., O'Keefe, J.M.K., 2015. Geochemical and mineralogical evidence for a coal-hosted uranium deposit in the Yili Basin, Xinjiang, northwestern China. Ore Geol. Rev. 70, 1–30.

Deng, J., Wang, Q.F., Gao, B.F., 2005. Evolution of ordos basin and its distribution of various energy resources. Geoscience 19 (4), 538–545 (in Chinese with English abstract).

Di, Y.Q., 2002. Preliminary discussion on prospecting potential for sandstone-type uranium deposits in Meso-Cenozoic basins, Northern Ordos. Uran. Geol. 18 (6), 340–347 (in Chinese with English abstract).

Ding, C., Chen, G., Li, Z.H., Mao, X.N., Yang, F., 2011. Apatite fission track analysis of tectono-thermal history in the Northeastern of Ordos Basin. Geoscience 25 (3), 581–588 (in Chinese with English abstract).

Fan, A.P., Liu, Y.Q., Yang, R.C., Feng, Q., Zhang, F.X., Han, Z.Z., 2007. Research on diagenesis of the sandstone-type uranium deposits in Dongsheng area, Ordos Basin. Sci China Ser D-Earth Sci 50, 195–202.

Fang, X.H., Li, Z.Y., 2017. Research on coffinite in Dongsheng uranium field. Uran. Geol. 33 (5), 257–265 (in Chinese with English abstract).

Feng, Z.B., Nie, F.J., Deng, J.Z., Zhang, H.J., Liu, B.H., 2017. Spatial-temporal collocation and genetic relationship among uranium, coal, and hydrocarbons and its significance for uranium prospecting: a case from the Mesozoic-Cenozoic uraniferous basins, North China. Russ. Geol. Geophys. 58, 611–623.

Feng, Q., Qin, Y., Fu, S.T., Liu, Y.Q., Zhou, D.W., 2016. The enrichment of calcite and the genesis of uranium deposits in Dongsheng Uranium Sandstone. Geol. J. China Univ. 1, 53–59 (in Chinese with English abstract).

Fishman, N.S., Reynolds, R.L., Robertson, J.F., 1985. Uranium mineralization in the Smith Lake District of the grants uranium region New Mexico. Econ. Geol. 80, 1348–1364.

Fleet, A.R., 1984. Aqueous and sedimentary geochemistry of the rare-earth elements. In: Henderson, P. (Ed.), Rare-Earth Element Geochemistry. Elsevier, London, pp. 331–373.

Gao, F., Pang, Y.Q., Zhao, L., Li, W.L., Ye, S.X., Fu, S.C., 2015. Study on occurrence of uranium mineral in Changjiang granite type Uranium Deposits of Zhuguang. Uran. Geol. 31 (A1), 330–335 (in Chinese with English abstract).

Guo, Z.M., Yu, Z.P., 1990. Structureal characteristics, mechanism of evolution and petroleum prospecting of Hetao Graben System. Petrol. Explor. Dev. 17 (3), 11–20 (in Chinese with English abstract).

Hall, S.M., Mihalasky, M.J., Tureck, K.R., Hammarstrom, J.M., Hannon, M.T., 2017. Genetic and grade and tonnage models for sandstone-hosted roll-type uranium deposits, Texas Coastal Plain, USA. Ore Geol. Rev. 80, 716–753.

Hou, B.H., Keeling, J., Li, Z.Y., 2017. Paleovalley-related uranium deposits in Australia and China: a review of geological and exploration models and methods. Ore Geol. Rev. 88, 201–234.

Hou, H.Q., Li, Y.R., Liu, H.J., Han, S.Y., Wang, G., Bai, Y.S., Wu, D., Wu, B.L., 2016. The organic matter characteristics of the Zhiluo formation and its relationship with uranium mineralization in the North Ordos Basin. Acta Geol. Sin. 90 (12), 3367–3374.

Hu, X.L., Gong, Y.J., Zeng, G.P., Zhang, Z.J., Wang, J., Yao, S.Z., 2018. Multistage pyrite in the Getang sediment-hosted disseminated gold deposit, southwestern Guizhou Province, China: Insights from textures and in situ chemical and sulfur isotopic analyses. Ore Geol. Rev. 99, 1–16.

Ingham, E.S., Cook, N.J., Cliff, J., Ciobanu, C.L., Huddleston, A., 2014. A combined chemical, isotopic and microstructural study of pyrite from roll-front uranium deposits, Lake Eyre Basin South Australia. Geochim. Cosmochim. Acta 125, 440–465.

Jiao, Y.Q., Chen, A.P., Wang, M.F., Wu, L.Q., Yuan, H.T., Zhang, C.Z., Xu, Z.C., 2005. Genetic analysis of the bottom sandstone of Zhiluo Formation, Northeastern Ordos Basin: Predictive base of spatial orientation of sandstone-type uranium deposit. Acta Sedimentol. Sin. 3 (3), 371–379 Doi. 1000-0550(2005)03-0371-09 (in Chinese with English abstract).

Jiao, Y.Q., Wu, L.Q., Peng, Y.B., Rong, H., Ji, D.M., Miao, A.S., Li, H.L., 2015. Sedimentary-tectonic setting of the deposition-type uranium deposits forming in the Paleo-Asian tectonic domain, North China. Geosci. Front. 22 (1), 189–205 (in Chinese with English abstract).

Jiao, Y.Q., Wu, L.Q., Rong, H., 2018. Model of inner and outer reductive media within uranium reservoir sandstone of sandstone-type uranium deposits and its ore-controlling mechanism: case studies in Daying and Qianjiadian Uranium Deposits. Earth

Sci. 2, 459–474 (in Chinese with English abstract).
Jin, R.S., Yu, R.A., Yang, J., Zhou, X.X., Teng, X.M., Wang, S.B., Si, Q.H., Zhu, Q., Zhang, T.F., 2019. Paleo-environmental constraints on uranium mineralization in the Ordos Basin: evidence from the color zoning of U-bearing rock series. Ore Geol. Rev. 104, 175–189.
Kalatha, S., Economou-Eliopoulos, M., 2015. Framboidal pyrite and bacterio-morphic goethite at transitional zones between Fe-Ni-laterites and limestones: evidence from Lokris, Greece. Ore Geol. Rev. 65, 413–425.
Li, Z.Y., Fang, X.H., Chen, A.P., Ou, G.X., Xiao, X.J., Sun, Y., Liu, C.Y., Wang, Y., 2007. Genesis of grey-green sandstone in the target strata of sandstone-type uranium deposits in northern Ordos Basin. Sci. China (Ser. D:Earth Sci.) 37 (Suppl.), 139–146 (in Chinese without English abstract).
Li, Z.Y., Chen, A.P., Fang, X.H., Ou, G.X., Xia, Y.L., Sun, Y., 2008. Origin and superposition metallogenic model of the sandstone-type uranium deposit in the northeastern Ordos Basin, China. Acta Geol. Sin. 82 (4), 745–749 (in Chinese with English abstract).
Li, X.D., Yi, C., Gao, H.W., Chen, X.L., Zhang, K., Wang, M.T., 2016. Study on formation mechanism of epigenetic altered zone in Zhiluo Formation, Northeastern Ordos Basin, North China. Geoscience 30 (4), 739–747 (in Chinese with English abstract).
Li, S.Z., Zhao, G.C., Dai, L.M., Liu, X., Zhou, L.H., Santosh, M., Suo, Y.H., 2012. Mesozoic basins in eastern China and their bearing on the deconstruction of the North China Craton. J. Asian Earth Sci. 47, 64–79.
Ling, M.X., Yang, X.Y., Sun, W., Miao, J.Y., Liu, C.Y., 2006. REE/trace element characteristics of sandstone-type uranium deposits in the Ordos Basin. Chin. J. Geochem. 25 (4), 354–364.
Liu, C.Y., 2005. Advances in the Accumulation and Formation for Multi-energy Mineral Deposits Coexisting in the Same Basin. Science Press, Beijing (in Chinese with English abstract).
Liu, Z.Y., Cai, G.Q., Dong, W.M., 2011. Sulfur isotopic characteristics in sulphides of typical uranium deposits in the Northern Tarim Basin and their geological significance. Acta Mineral. Sin. 31 (A1), 619–620 (in Chinese without English abstract).
Liu, J.J., Feng, C.X., Zheng, M.H., 2001. Advances in selenium resources study. World Sci.-Technol. R & D. 23 (5), 16–21 (in Chinese with English abstract).
Liu, Y.Q., Feng, Q., Yang, R.C., Fan, A.P., Xing, X.J., 2006c. Discussion on genesis of sandstone-type uranium deposits in Dongsheng Area, Ordos Basin. Acta Geol. Sin. 80 (5), 761–767 (in Chinese with English abstract).
Liu, H.B., Li, Z.Y., Qin, M.K., Sun, Y., Han, J., Jin, G.S., Li, J.J., 2012. Progress in geochemistry of sandstone-type uranium deposit in North Ordos Basin. Geosci. Front. 19 (3), 139–146 (in Chinese with English abstract).
Liu, J., Nie, F.J., Hou, S.R., Chen, L.L., Wang, J.L., 2013. Types of Uraniam Minerial and its occurrence state of the sandstone-type uranium deposits in the Meso-cenozoic Basin. J. East China Inst. Technol. 2, 107–112 (in Chinese with English abstract).
Liu, D.C., Ye, F.W., Zhao, Y.J., 2006b. Analyzing regional geological setting of DS uranium deposit based on the extensional research of remote sensing information. World Nucl. Geosci. 23 (4), 232–237 (in Chinese with English abstract).
Liu, C.Y., Zhao, H.G., Tan, C.Q., Wang, J.Q., 2006a. Occurrences of multiple energy mineral deposits and mineralization/reservoiring system in the basin. Oil Gas Geol. 27 (2), 131–142 (in Chinese with English abstract).
Liu, M.H., 2011. Occurrence and Origin of the Pyrite in Uranium Reservoir in Yijinhuoluo of Ordos Basin. Master's thesis. P31–50. (in Chinese with English abstract).
Ma, Y., Wu, B.L., Liu, Y.F., Liu, C.Y., Zhao, Z.P., Wang, H.T., Song, Z.S., Wei, A.J., 2013. Study on uranium occurrence state of sandstone-type uranium deposits in HJQ region, Ordos Basin. Northwestern Geol. 46 (2), 141–152 (in Chinese with English abstract).
Manuel, K., Daniel, J.S., Gawen, R.T.J., 2018. A review of Te and Se systematics in hydrothermal pyrite from precious metal deposits: Insights into ore-forming processes. Ore Geol. Rev. 96, 269–282.
Максимова, М.Ф., Шмариович, Е.М., 1993. Пластово-инфильтрационноерудообразование. М: Недра.
McLemore, V.T., 2010. The Grants Uranium DistrictNew Mexico: update on source, deposition, and exploration,. Mountain Geol. 48 (1), 23–44.
McLennan, S.M., 1989. Rare-earth elements in sedimentary rocks, influence of provenance and sedimentary processes. In: Lipin, B.R., McKay, G.A. (Eds.), Geochemistry and Mineralogy of Rare-Earth Elements. Min. Soc. Am. Rev. Mineral. pp. 169–200.
Miao, A.S., Lu, Q., Liu, H.F., Xiao, P., 2009. Occurrence and formation of coffinite in ancient interlayer oxidizing zone of sandstone type U-deposit in Ordos Basin. Geol. Sci. Technol. Inf. 4, 51–58 (in Chinese with English abstract).
Min, M.Z., Wu, Y.Y., Zhang, W.L., Zhang, G.H., Geng, J.H., 1999. A densely zoned rhythmically intergrowth of coffinite and pitchblende and its genetic significance. Acta Mineral. Sin. 19 (1), 15–19 (in Chinese with English abstract).
РафалъскийРП. 1963. Физико-химическоеИсследованиеУсловийОбразованияУрановыхРуд. Москва: Атомиздат. 56-123.
Peng, Y.B., Li, Z.Y., Fang, X.H., Jie, Q.L., 2006. Metallogenetic characteristics of No. 2081 uranium deposit in the North of Ordos Basin. Acta Mineral. Sin. 3, 349–355 (in Chinese with English abstract).
Qi, J.M., Luo, C.W., Huang, G.L., Cao, H.J., Xu, L.L., 2015. Geochemical character of pyrite and its tracing effects to ore-forming fluid for granite type uranium deposit in North Guangdong. Uranium Geol. 31 (2), 73–80 (in Chinese with English abstract).
Qiu, X., Liu, C., Mao, G., Deng, Yu, Wang, F., Wang, J., 2014. Late Triassic tuff intervals in the Ordos Basin, Central China: their epositional, petrographic, geochemical characteristics and regional implications. J. Asian Earth Sci. 80, 148–160.
Ren, Z.L., Zhang, S., Gao, S.I., Cui, J.P., Xiao, Y.Y., Xiao, H., 2007. Tectonic thermal evolution history of Ordos Basin and its significance of accumulation and mineralization. Sci. China (Ser. D:Earth Sci.) 37 (Suppl), 139–146 (in Chinese without English abstract).
Rollinson, H.R., 1993. Using Geothemical Data: Evaluation, Presentation. Longman Scientific Techical Press, London, Interpretation.
Seal, R.R., 2006. Sulfur isotope geochemistry of sulfide minerals. Rev. Mineral. Geochem. 61, 633–677.
Skirrow, G.R., Mercadier, J., Armstrong, R., Kuske, T., Deloule, E., 2016. The Ranger uranium deposit, northern Australia: timing constraints, regional and ore-related alteration, and genetic implications for unconformity-related mineralization. Ore Geol. Revi. 76, 463–503.
Song, H., Ni, S.J., Hou, M.C., Zhang, C.J., Shi, Z.Q., Wang, G., Yang, B., Hu, Y., Chen, Y.J., 2016. The characteristic of clay minerals in sandstone-type uranium deposit in the Yili Basin, NW China and its relationship with uranium mineralization. Acta Geol. Sin. 90 (12), 3352–3366 (in Chinese with English abstract).
Spirakis, C.S., 1996. The roles of organic matter in the formation of uranium deposits in sedimentary rocks. Ore Geol. Rev. 11 (1), 53–69.
Sun, Y., Li, Z.Y., Xiao, J.X., Hou, G.W., 2004. Relationship between oil-gas trap and uranium metallogenesis at northern Ordos basin. Uranium Geol. 20 (6), 337–343 (in Chinese with English abstract).
Sun, L.X., Zhang, Y., Zhang, T.F., Cheng, Y.H., Li, Y.F., Ma, H.L., Yang, C., Lu, C., Zhou, X.G., 2017. Jurassic sporopollen of Yan'an Formation and Zhiluo Formation in the northeastern Ordos Basin, Inner Mongolia, and its paleoclimatic significance. Earth Sci. Front. 24 (1), 32–51 (in Chinese with English abstract).
Tu, G.Z., Gao, Z.M., 2003. Ore-forming mechanism of the dispersed elements. Bull.Chin. Acad. Sci. 18 (5), 358–361 (in Chinese with English abstract).
Turner-Peterson, C.E., 1985. Lacustrine-humate model for primary uranium ore deposits, grants uranium region, New Mexico. Am. Assoc. Petrol. Geol. Bull. 69 (11), 1999–2020.
Wang, S.M., 2017. Ordos Basin superposed evolution and structural controls of coal forming activities. Earth Sci. Front. 24 (2), 54–63 (in Chinese with English abstract).
Wang, J., Du, L.T., 1995. Gas reduction: an important factor in the formation of uranium deposits. Uranium Geol. 11 (1), 19–24 (in Chinese with English abstract).
Wang, G., Wang, Q., Miao, A.S., Jiao, Y.Q., Yi, C., Zhang, K., 2017. Characteristic of uranium minerals in Nalinggou Uranium Deposit of ordos basin and their formation mechanism. ACTA Mineral. Sin. 37 (4), 461–468 (in Chinese with English abstract).
Webster, J.D., 1983. Petrography of some Ambrosia Lake, New Mexico, prefault uranium ores, and implications for their genesis: USGS Open-File Report. 83-8, 72 p.
Wu, B.L., Liu, C.Y., Zhang, F.X., Fang, X.H., Liu, X., 2006. Geochemical Characteristics of Epigenetic Alteration in Dongsheng Sandstone-type Uranium Deposit and its Metallogenic Signification. ATCA Geol. Sin. 80 (5), P740–747 (in Chinese with English abstract).
Wu, B.L., Liu, C.Y., Wang, J.Q., 2007. Basical characteristics of fluid geologic process of interlayer oxidation zone sandstone-type uranium deposit. Sci. China Ser. D-Earth Sci. 50 (Suppl. 2), 185. https://doi.org/10.1007/s11430-007-6016-z.
Wu, B.L., Wei, A.J., Liu, C.Y., Song, Z.S., Hu, L., Wang, D., Cun, X.N., Sun, L., Luo, J.J., 2015. Stable isotope tracing on the formation of white sandstone in Yan'an Group, Northern Ordos Basin, and its geological significance. Earth Sci. Front. 22 (3), 205–214 (in Chinese with English abstract).
Wu, B.L., Zhang, Y.W., Song, Z.S., Cun, X.N., Sun, L., Luo, J.J., Li, Y.Q., Cheng, X.H., Sun, B., 2016. Geological and Geochemical Characteristics of Uranium Minerals in the Sandstone-type Uranium Deposits in the North of Ordos Basin and Their Genetic Significance. Acta Geol. Sin. 90 (12), 3393–3407 (in Chinese with English abstract).
Xia, Y.L., Lin, J.R., Liu, H.B., Fan, G., Hou, Y.X., 2003a. Research on geochronology of sandstone-hosted uranium ore-formation in major uranium-productive basins, northern China. Uranium Geol. 19 (3), 129–136 (in Chinese with English abstract).
Xia, Y.L., Liu, H.B., 2005. Pre-enrichment and metallogeny of uranium in Zhiluo Formation sand bodies of Dongsheng area, Ordos Basin. World Nucl. Geosci. 22 (4), 187–191 (in Chinese with English abstract).
Xia, Y.L., Lin, J.R., Liu, H.B., Fan, G., Hou, Y.X., 2003b. Research on geochronology and uranium source of sandstone-hosted uranium ore-formation in major uranium-productive basins, Northern-China. China Nucl. Sci. Technol. Rep. 2, 80–90 (in Chinese with English abstract).
Xiang, W.D., Fang, X.H., Li, T.G., Chen, X.L., Pang, Y.Q., Cheng, H.H., 2006a. Metallogenic characteristics and model of Dongsheng uranium deposit in Ordos basin, North China. Uranium Geol. 22 (5), 257–266 (in Chinese with English abstract).
Xiang, W.D., Chen, X.L., Pang, Y.Q., Fang, X.H., Li, G.T., 2006b. Mineralogical and geochemical characteristics and genetic mechanism of gray-greenish alteration sandstone of the Dongsheng uranium deposit in the Ordos basin, North China. Miner. Deposits. 25 (A1), 261–264 (in Chinese with English abstract).
Xiang, W.G., 2009. InvestigatiInvestigation on Performance of Gasification CLC Combined Cycle and on CLC Characteristics using Iron Oxide as Oxygen Carrier. Doctor's Thesis. PI-II. (in Chinese with English abstract).
Xing, X.J., Liu, Y.Q., Fan, A.P., 2006. Genesis of sandstone-type uranium deposits: a case study in the Diantou area of the Ordos basin. Geol. China 33 (3), 591–597.
Xing, X.J., Liu, Y.Q., Li, W.D., Long, B.L., 2008. Sandstone diagenesis and uranium mineralization of the Zhiluo Formation in the Diantou Area, Southern Ordos Basin. Acta Geosci. Sin. 29 (2), 179–188 (in Chinese with English abstract).
Xue, C.J., Chi, G.X., Xue, W., 2010. Interaction of two fluid systems in the formation of sandstone-hosted uranium deposits in the Ordos Basin: geochemical evidence and hydrodynamic modelling. J. Geochem. Explore 106, 226–235.
Xue, C., Feng, Q., Tian, H., 2011. Distribution and prospect of oil sand resources in China. Xinjiang Petrol. Geol. 32 (4), 348–350 (in Chinese with English abstract).
Yang, X.K., Chao, H.X., Volkova, N.I., Zheng, M.L., Yao, W.H., 2009a. Geochemistry and SHRIMP geochronology of alkaline rocks of the Zijinshan massif in the eastern Ordos basin, China. Russ. Geol. Geophys. 50 (9), 751–762.
Yang, M.H., Li, L., Zhou, J., Qu, X.Y., Zhou, D., 2013. Segmentation and inversion of the Hangjinqi fault zone, the northern Ordos basin (north China). J. Asian Earth Sci. 70

(71), 64–78.
Yang, M.H., Li, L., Zhou, J., Jia, H.C., Sun, X., Qu, X.Y., Zhou, D., Gong, T., Ding, C., 2015. Mesozoic structural evolution of the Hangjinqi area in the northern Ordos Basin, North China. Marine Petrol. Geol. 66 (4), 695–710.
Yang, X.Y., Luo, X.D., Ling, M.X., Lai, X.D., 2008. Geochemical features of sandstone-type uranium deposits in the ordos basin and their geological significances. Geol. Rev. 54 (4), 539–549 (in Chinese with English abstract).
Yang, X.Y., Ling, M.X., Lai, X.D., Sun, W., Liu, C.Y., 2009b. Uranium mineral occurrence of sandstone-type uranium deposits in the Dongsheng-Huanglong Region, Ordos Basin. Acta Geol. Sin. 8, 1167–1177 (in Chinese with English abstract).
Yang, B.H., Luo, J.L., Dai, Y.Q., Liu, X.H., Lin, T., Zhang, S., 2006. Petrology of uranium-bearing sandstones and relationship of organic matters, hydrocarbons and coal with uranium: an example from Dongsheng, Ordos Basin and Shihongtan, Tuha Basin. J. Northwest Univ.(Nat. Sci. Ed.) 36 (6), 982–991 (in Chinese with English abstract).
Yuan, Y.S., Hu, S.B., Wang, H.J., Sun, F.J., 2007. Meso-Cenozoic tectonothermal evolution of Ordos basin, central China: Insights from newly acquired vitrinite reflectance data and a revision of existing paleothermal indicator data. J. Geodyn. 44, 33–46.
Zhang, J.D., 2016. Innovation and development of metallogenic theory for sandstone type uranium deposit in China. Uran. Geol. 32 (60), 321–332 (in Chinese with English abstract).
Zhang, C., Chao Yi, C., Dong, Q., Cai, Y.Q., Liu, H.X., 2018. Geological and geochronological evidence for the effect of Paleogene and Miocene uplift of the Northern Ordos Basin on the formation of the Dongsheng uranium district, China. J. Geodyn. 114, 1–18.
Zhang, L., Liu, C.Y., Zhao, Z.P., Wang, F.F., Song, Z.S., 2015. Fluid evolution and mineralization of Hangjinqi sandstone-type uranium deposit, Ordos Basin. Earth Sci. Front. 3, 368–381 (in Chinese with English abstract).
Zhang, L., Liu, C.Y., Lei, K.Y., Sun, L., Cun, X.N., Du, F.P., Deng, H., 2017b. White bleached sandstone genesis and paleo-weathered crust forming environment of the Jurassic Yanan formation in the northeastern ordos basin. Acta Geol. Sin. 91 (6), 1345–1359 (in Chinese with English abstract).
Zhang, L., Liu, C.Y., Mostafa, F., Wu, B.L., Lei, K.Y., Cun, X.N., Sun, L., 2017a. Hydrothermal mineralization in the sandstone–hosted Hangjinqi uranium deposit, North Ordos Basin, China. Ore Geol. Rev. 80, 103–115.
Zhang, F.X., Qiao, H.M., Jia, H., 2006. The metallogenic condition and epigenetic alteration mineralization of Dongsheng uranium deposit in the inner Mongolia. Acta Geol. Sin. 80 (5), 733–739 (in Chinese with English abstract).
Zhang, T.F., Sun, L.X., Zhang, Y., Cheng, Y.H., Li, Y.F., Ma, H.L., Lu, C., Yang, C., Guo, G.W., 2016b. Geochemical characteristics of the Jurassic Yan'an and Zhiluo formations in the northern margin of Ordos Basin and their paleoenvironmental implications. Acta Geol. Sin. 90 (12), 3454–3472 (in Chinese with English abstract).
Zhao, L., Cai, C.F., Jin, R.S., Li, J.G., Li, H.L., Wei, J.L., Guo, H., Zhang, B., 2018c. Mineralogical and geochemical evidence for biogenic and petroleum-related uranium mineralization in the Qianjiadian deposit, NE China. Ore Geol. Rev. 101, 273–292.
Zhao, H.L., Chen, L.L., Feng, X.X., Li, J.G., Chen, Y., Wang, G., 2018a. Features of clay minerals in the middle Jurassic Zhiluo formation sandstones of the Nalinggou Area in the Ordos Basin and a preliminary comparison with adjacent areas. Geol. J. China Univ. 24 (5), 627–636.
Zhao, Z.Y., Guo, Y.R., Wang, Y., Lin, D.J., 2012. Study progress in tectonic evolution and paleogeography of Ordos Basin. Spec. Oil Gas Reservoirs 19 (5), 15–21 (in Chinese with English abstract).
Zhao, W.T., Hou, G.T., Hari, K.R., 2016. Two episodes of structural fractures and their stress field modeling inthe Ordos Block, northern China. J. Geodyn. 97, 7–21.
Zhao, J., Liang, J.L., Long, X.P., Li, J., Xiang, Q.R., Zhang, J.C., Hao, J.L., 2018b. Genesis and evolution of framboidal pyrite and its implications for the ore-forming process of Carlin-style gold deposits, southwestern China. Ore Geol. Rev. 102, 426–436.
Zhao, J.F., Mountney, Nigel P., Liu, C.Y., Qu, H.J., Lin, J.Y., 2015. Outcrop architecture of a fluvio-lacustrine succession: Upper Triassic Yanchang Formation, Ordos Basin, China. Mar. Pet. Geol. 68, 394–413.
Zheng, Y.F., Chen, J.F., 2000. In: Stable Isotope Geochemistry. Science Press, Beijing, pp. P218–247.
Zhou, J., Qiu, Z., Wang, H.Y., Lu, B., Bai, W.H., Liu, D.X., Tan, X., Jiang, Z.H., 2017. Formation mechanism of pyrite framboid and its research significance. Chin. J. Geol. 52 (1), 242–253 (in Chinese with English abstract).
Zhou, J.Y., Zheng, R.C., Zhu, Z.M., Chen, J.B., Shen, B., Li, X.Y., Luo, L.P., 2008. Geochemical characteristics of trace elements of pyrite and its implication to the metellogenesis in the Lala Copper Deposit. J. Mineral. Petrol. 28 (3), 64–71 (in Chinese with English abstract).
Zou, M.L., Huang, H.Y., Liu, X.Y., Fan, L.T., Xiang, T.F., Xu, H., Ouyang, P.N., 2017. Characterization of arsenic-bearing pyrite and the relationship with uranium metallogenic in the Central Zhuguang Pluton, Southern China. Geol. Rev. 63 (4), 1021–1039 (in Chinese with English abstract).
Zou, H.P., Zhang, K., Li, G., 2008. Cretaceous tectono-thermal event in the ordos block: an Ar-Ar chronological evidence from basalt at Hang Jin Banner, Inner Mongolia, North China Craton. Geotectonica Metall. 32 (3), 360–364 (in Chinese with English abstract).
ДамковЮ М. 1973. ПрироцаУрановойРудыВопросы,ГенетическойМинералогии. Москва: Атомиздат. 53-68.
КомовИЛ. 1982. РадиационнаяМинерол.Москва: Знергоиздат. 156-178.